Physics – Uspekhi **63** (9) 888 – 906 (2020)

REVIEWS OF TOPICAL PROBLEMS PACS numbers: **02.70. – c**, **34.35. + a**, 73.20.At, 73.40.Gk, **73.63. – b**, 79.20.Rf

Resonant charge transfer during ion scattering on metallic surfaces

I K Gainullin

DOI: https://doi.org/10.3367/UFNe.2019.11.038691

Contents

Abstract. Electron transfer during low-energy ion scattering (LEIS) is discussed in the article. In most cases, the final charge state of ions/atoms scattered from a metallic surface is formed due to resonant charge transfer (RCT). The key concepts, model representations, and basic laws of electronic exchange are systemized in the article. For practical usage, RCT is primarily important for surface diagnostics by LEIS, because incorrectly taking into account electronic exchange can lead to significant errors. It is noteworthy, that LEIS has the best surface sensitivity and is indispensable for diagnosing the composition of the upper surface layer.

Keywords: ion beams, scattering, metals, nanosystems, charge (electronic) exchange, resonant charge transfer, surface analysis

1. Introduction

Ion beams are widely used in solid-state diagnostics, the controlled modification of surface properties, creating functional coatings, the treatment of oncological diseases, and solving other problems related to the analysis and modification of properties of physical objects at the atomic level [1–12].

I K Gainullin Lomonosov Moscow State University, Faculty of Physics, Leninskie gory 1, build. 2, 119991 Moscow, Russian Federation
E-mail: Ivan.Gainullin@physics.msu.ru

Received 21 May 2019, revised 5 November 2019
Uspekhi Fizicheskikh Nauk **190** (9) 950 – 970 (2020)
Translated by V L Derbov

Physical processes that occur during the interaction of ions with a solid are commonly divided according to the form of energy transfer into elastic and inelastic (in which the kinetic energy of the system is not conserved). Elastic processes include ion scattering, sputtering of surface atoms, and modification of the crystal lattice of the solid. Inelastic processes are characterized by interaction with the electron subsystem of the solid, including electron exchange, emission of electrons, and deceleration of ions because of the excitation of the electronic system.

A general layout of surface studies and modification using ion beams is presented in Fig. 1a. Experimental studies are carried out under conditions of high and superhigh vacuums ($10^{-9} – 10^{-11}$ Torr). Note that since the surface is irradiated with charged particles (mainly single-charged positive ions) it is common to speak of ion–surface interaction. However, the physics of interaction with a surface will be similar for neutral atoms as well. Therefore, in the context of charge transfer, we speak about the interaction of atomic particles with a surface, where an atomic particle can be either a neutral atom or a single-charged positive (or negative) ion.

Figure 1b shows a photograph of a setup for experimental investigation of interaction of ion beams with a surface. To maintain a high vacuum, up-to-date setups consist of metallic modules. The basic modules are the analytic chamber in which the sample under study is placed, the source of ions and ion optics for controlling the parameters of the primary beam, and the pumping system. In experiments aimed at modifying the surface composition and structure by ion beams, the analysis of exposed samples is, as a rule, carried out using other instruments (e.g., electron and atomic-force microscopes). However, the study of surface properties by

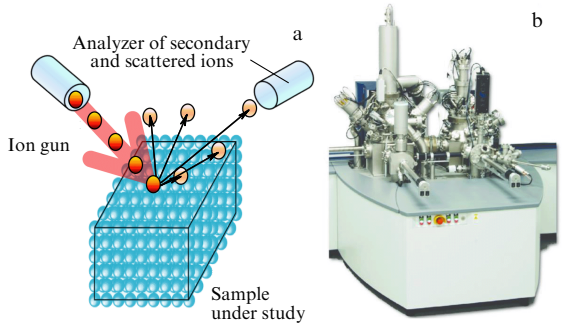

Figure 1. (a) General layout of surface diagnostics using ion beams. (b) Photograph of super-high vacuum TOF.SIMS 5 and Qtac 100 setup for surface composition diagnostics.

means of scattering or sputtering of ions requires additional instruments to detect and analyze the scattered and sputtered atoms/ions, which substantially complicates the setup construction.

The scope of this review is restricted to metallic surfaces, since the electron exchange with them is substantially more deeply studied both experimentally and theoretically, and the existing computational theoretical models in many cases quantitatively describe experimental dependences [8, 13]. For most elements of the periodic table (except neutralization of positive ions of inert gases), the electron exchange with metallic surfaces occurs in a resonant way.

The electron exchange between atomic particles and a surface is essential in quantitative diagnostics of the elemental composition and structure of solids. In most experimental setups, it is exactly the ions that are detected, and their spectra are determined by the cross section of elastic scattering or sputtering and the neutralization probability, i.e., by electron exchange. The electron exchange between atomic particles and the surface plays an important role in both the ion scattering and the sputtering of surface atoms. However, the experimental investigation of electron transfer, as a rule, is carried out exactly for ion scattering, since, in this case, it is possible to choose the type of primary ions, to vary their energy and direction of incidence, and to determine the probability of electronic transition from the ratio of charged/neutral scattered atomic particles. Note that the electron exchange processes are of primary importance for low-energy ions (with the energy of a few keV or lower). Moreover, low-energy ion scattering (LEIS) is the only method that allows analyzing the elemental composition of the first surface layer [14, 15].

Section 2 considers the basic concepts and methods of investigating electron exchange between atomic particles and a surface. In Section 3, we describe the lines of electron exchange investigation, the main known results, and actual problems. The emphasis is on the interpretation and computational-theoretical explanation of experimental results. Section 4 contains a description of the practical use of electron exchange and examples of surface elemental composition analysis by LEIS methods.

For convenience, by default we use the atomic system of units, in which $m_e = e = \hbar = 1$, 1 a.u. of length $= 0.53$ Å, 1 a.u. of time $= 2.419 \times 10^{-17}$ s, and 1 a.u. of velocity $= 2.188 \times 10^8$ cm s^{-1}. The energy, as a rule, is presented in electron-volts. In the figures, the experimental data are shown by symbols (marks) and the calculated results by lines.

2. Basic concepts and methods of study of electron exchange

2.1 Classification of electron exchange processes: basic concepts and models

2.1.1 Classification of electron exchange processes. In the scientific literature [13], the following kinds of electron exchange between atomic particles and a surface are considered (Fig. 2):

(1) Resonant charge transfer (resonant ionization and neutralization) — electron exchange with the conduction band with conservation of the electron energy. The formation of an equilibrium charge state of the atomic particle under resonant electron exchange with metals occurs at characteristic distances of 5–10 a.u. from the surface.

(2) Auger processes — two-electron processes, in which the energy released due to a transition of one electron is transferred to another. Auger capture of an electron by a positive ion (Auger neutralization) and Auger relaxation (Auger deexcitation) of an excited neutral atom are most common. Auger ionization of a neutral atom is relatively rare. Auger processes occur at a characteristic distance of 2–4 a.u. from the surface. In the case of multiply charged ions, this distance can increase up to dozens of atomic units.

(3) Quasi-resonant electron exchange with a deep (bound) energy level that occurs in some combinations of metals (Pb, Au) and inert gas ions (He^+, Ne^+).

(4) Quasi-resonant electron exchange directly during a collision with a lattice atom (collision-induced reionization/neutralization). It takes place at distances of up to 1 a.u. from the surface due to overlapping of electronic states of an atomic particle and a lattice atom. It is important in electron exchange with dielectric surfaces.

(5) Nonresonant electronic transition — a single-electron transition with a change in electron energy. The probability of nonresonant transitions is small compared to resonant ones; therefore, they are not typically considered in the case of ions interacting with a surface.

2.1.2 Basic concepts of electron exchange. In the theoretical description of electron exchange between atomic particles and a surface, the concept of an *active electron* and a *frozen atomic core* actively exploited in atomic physics is commonly used. Electron exchange is considered with a single definite active state (energy level) of the atomic particle electron. In this concept, the atomic particle is considered a single-electron hydrogen-like quasi-atom consisting of a 'frozen' core and an active electron participating in the electron exchange. For

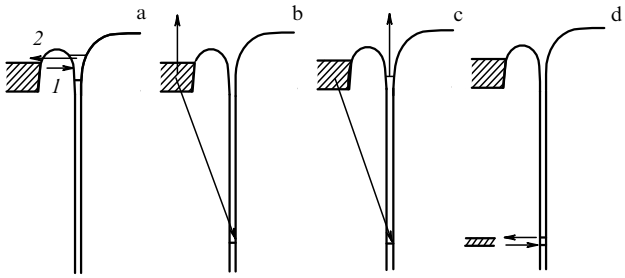

Figure 2. Illustration of different kinds of electron exchange: (a) resonant, (b) Auger capture, (c) Auger deexcitation, (d) quasi-resonant exchange with a deep energy level.

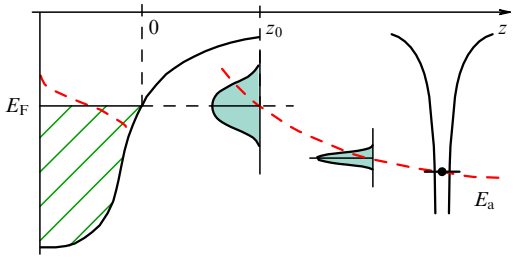

Figure 3. Illustration of the energy position change and energy level broadening in an atomic particle approaching a surface.

instance, when considering the loss of an electron by a neutral atom or the capture of an electron by a positive ion, the role of the core is played by the appropriate positive ion. For the loss of an electron by a negative ion or the capture of an electron by a neutral atom, the core is the neutral atom itself.

The key concept of electron exchange between atomic particles and a surface is *atomic particle energy position* or *energy level*. The energy position of an atomic particle equals the energy of the active electron localized on it. For example, the energy position of a positive ion with respect to the vacuum energy level is equal to the ionization energy of the corresponding neutral atom. The energy position determines the possibility and direction of electronic transitions (see Section 2.1.3.1 below). It should be noted that in the case of metallic surfaces the energy position depends on the distance from the surface due to the interaction with image charges (see Section 2.1.3.2).

If an atomic particle is located near a metal surface, the wave functions of electrons in the metal and in the atomic particle overlap. In terms of quantum mechanics, the metal perturbs the active energy level $|a\rangle$ of the atomic particle, and vice versa, the electron states $|k\rangle$ in the metal are perturbed by the atomic particle. According to the Heisenberg uncertainty relation, the lifetime τ of a state $|a\rangle$ is expressed as $\tau\Gamma \approx 1$, where Γ is the *energy level width* of the atomic particle, which determines the efficiency of the electron exchange between the atomic particle and the surface. In the first approximation, the energy level width is determined by the Fermi 'golden rule'

$$\Gamma = 2\pi \sum_{\mathbf{k}} \rho(E_a) \left|\langle a|V|k\rangle\right|^2 , \qquad (1)$$

where ρ is the density of electronic states in the metal, E_a is the energy level of the atomic particle, and V is the perturbation operator.

Figure 3 illustrates the change in the energy position (see Section 2.1.3.2) and the broadening of the energy level in a positive ion approaching a metallic surface.

2.1.3 Basic model concepts of electron exchange. In this section, we present the basic model concepts of electron exchange, obtained from the interpretation of experimental data. Mechanisms of neutralization of positive ions of alkali metals, neutralization of positive ions of inert gases, and the formation of negative ions are considered separately.

2.1.3.1 Conditions for implementing different electron exchange processes. The possibility and probability of different electron exchange processes are determined by the energy band structure of a solid and the energy position of an atomic particle (Fig. 4). For metals, if the energy level of an atomic particle is higher than the metal Fermi level, then the

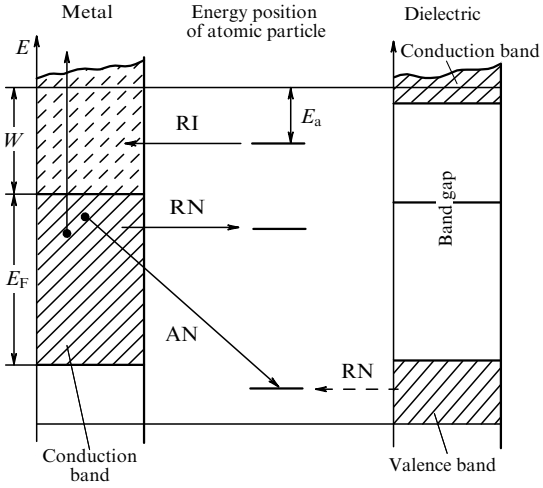

Figure 4. Comparative illustration of electron exchange with metals and dielectrics. RI — resonant ionization (loss of an electron by a neutral atom), RN — resonant neutralization (capture of an electron by a positive ion), AN — Auger neutralization.

resonant transfer of an electron from the atomic particle to the surface is possible, but not vice versa (because electronic states above the Fermi level are not filled). Conversely, if the ion energy level is below the Fermi level of the metal, a resonant transfer of an electron from the surface to the ion is possible (while the reverse transition is forbidden, as all the states below the Fermi level are filled). Since the resonant transition is single-electron, its probability is substantially higher than those of two-electron Auger processes [13]. Auger processes play an essential role only in the scattering of ions of inert gases, whose energy position is lower than the conduction band bottom (i.e., when a resonant transition is impossible).

For dielectrics, resonant neutralization of a positive ion is possible if its energy level is located against a filled band. No resonant ionization (loss or capture of an electron by a neutral atom) occurs, because the energy position of the atomic particle corresponds to a band gap. Auger processes in the interaction of ions with dielectrics are possible if the released energy exceeds the band gap width. For semiconductors (a band gap width of the order of 1 eV), all kinds of electron exchange can occur.

Quasi-resonant exchange with a deep-lying energy level is observed in the scattering of inert gas ions by some metals. It is characterized by an oscillating dependence of electron yield on the velocity of electrons. These oscillations of the charge state of the scattered ions have a quantum mechanical nature. In atomic physics, they are known as Stückelberg oscillations [16] and are explained by means of the Landau–Zener model. The quasi-resonant exchange with a deep level is observed only in some combinations of ions of inert gases (He^+, Ne^+) and metallic surfaces (Pb, Au).

Quasi-resonant electron exchange directly during a collision with a lattice atom occurs in the case of both metal and dielectric surfaces. However, for metal surfaces, the formation of the final charge state occurs during the rebound of the atomic particle from the surface at the expense of resonant processes (see memory loss effect in Section 2.1.3.3).

We should emphasize that among all elements of the periodic table the most interesting in view of electron transfer investigation are exactly the ions of alkali metals and inert

gases [17]. This is because the energy level of the remaining elements of the periodic table (ionization energy 5–15 eV) is located against the filled part of the conduction band, so that the probability of resonant neutralization of such ions is almost 100%. Therefore, the study of electron exchange with such elements is not very informative. Note that for the sputtering of surface atoms a typical yield of charged particles is only 0.1%. The energy position of inert gas ions (ionization energy 15–24 eV), as a rule, crosses the bottom of the conduction band of metals. Therefore, because of resonant neutralization and Auger processes, the probability of neutralization for inert gas ions amounts to 90% and higher (up to 99%). The energy position of alkali metal ions (ionization energy 4.3–5.4 eV), as a rule, crosses the Fermi level of metals. Therefore, for alkali metals, the resonant processes of both loss and capture of an electron are realized, and the probability of neutralization amounts to dozens of percent. Hence, the alkali metal ions are the most informative for studying the resonant charge transfer. The advantage of LEIS with alkali metal ions is that the typical probability of alkali metal ion neutralization is about 10%, whereas for inert gases it exceeds 90%. Therefore, the signal of scattered alkali metal ions turns out to be greater by almost an order of magnitude, which allows reducing the exposure dose and preventing surface destruction [18]. It is exactly for this reason that alkali metal ions are frequently used to analyze the crystal structure of surfaces that require angular scanning [19, 20].

2.1.3.2 Change of energy position of an atomic particle due to interaction with an image charge. Due to interactions with image charges, the energy position of an atomic particle near a metallic surface shifts by [21, 22]

$$\Delta E_a = \frac{\langle \varphi_a | H_p | \varphi_a \rangle}{\langle \varphi_a | \varphi_a \rangle} \approx \frac{2Z-1}{4R}, \quad (2)$$

where H_p is the Hamiltonian acting on an active electron, φ_a is the wave function of the active electron, Z is the atomic core charge (can be positive, zero, or negative), and R is the distance to the plane of the induced charge localization (so-called imaginary plane). Thus, the energy position of a neutral atom (positive atomic core) rises approximately as $E_a(z) \approx E_a(\infty) + 1/4z$, when approaching the surface (see Fig. 3). For a negative ion (neutral atomic core), the energy position descends approximately as $E_a(z) \approx E_a(\infty) - 1/4z$, where $z = R$ is the distance to the 'imaginary' plane. This issue is considered in more detail in Section 3.3 of review [13], including the asymptotic dependence of the energy position on the distance near the surface.

References [23, 24] consider the response of a solid surface to a moving charge. From the derived analytical expressions for the potential of interaction with the induced charge, it follows that the classical concept of the image charge is applicable both to the scattering of low-energy ions and to the grazing-incidence scattering of fast ions if the normal component of the velocity is less than 0.5 a.u. Note that the velocity of 0.5 a.u. corresponds to a hydrogen atom kinetic energy of about 6 keV, or a few dozen keV for heavier atomic particles.

2.1.3.3 Effect of loss of memory of the initial charge state. The loss of memory of the initial charge state is extremely important for modeling experiments on electron exchange. The essence of the effect is as follows. Under LEIS on metal surfaces, the final charge state of an atomic particle is formed when moving off the surface and is independent of the initial charge state, energy, and angle of incidence of the primary beam, as well as the trajectory of atomic particle motion in the immediate vicinity of the surface.

The memory loss effect is confirmed by a number of experimental studies. For example, in Ref. [25], the yield fraction of H^- ions under scattering on an Al surface was measured at different charge states of the primary beam (H^+ and H^-) and for different ion exit angles (from 0° to 40° with respect to the surface). It was shown that the final charge state does not depend on the initial one in a wide range of the ion exit angles.

In another experiment demonstrating the memory loss effect, the probability of neutralization of Li^+ ions on a Cu(111) surface was measured at a fixed normal component of the exit energy of scattered ions and different energies and incidence angles of the primary beam. The neutralization probability amounted to nearly 25% and was independent of the incidence angle and primary beam energy.

The memory loss effect is explained as follows. Near a metal surface ($z < 3$ a.u.), the efficiency of electron transfer is so high that the charge state of an atomic particle quickly comes to an equilibrium value, which depends neither on its initial charge state nor on the primary beam parameters (energy, angle of incidence) and the trajectory of the atomic particle motion near the surface. The formation of the final charge state occurs during the departure of the atomic particle from the surface at distances $z > 3$ a.u., as a rule, due to resonant electronic transitions.

2.1.3.4 Kinematic effect (parallel velocity effect). It is worth noting that at high velocities of atomic particles (0.2 a.u. and higher) resonant electronic processes are affected by the so-called *kinematic effect*. The kinematic effect most clearly manifests itself in grazing-incidence scattering experiments, because they provide a relatively long duration of ion–surface interaction at high velocities. For this reason, it is also referred to as the *parallel velocity effect*, and electron transfer under grazing-incidence scattering is considered a separate branch of ion–surface interaction studies.

The basic idea is to recast the wave functions of conduction band electrons to the reference frame of the moving ion. The Galilean transformation is widely used to study collisions of fast atoms and ions [26, 27]. Based on the concept of the electron translation factor, it can be shown that in the reference frame of a moving atomic particle one can use the 'static' wave functions of the metal shifted in the k-space by the value of the parallel component of the atomic particle velocity [28]. We recall that the wave vector and velocity dimensions coincide in the atomic system of units.

In the fixed metal reference frame, all electrons are inside the so-called Fermi sphere, and $k_F^2/2$ is the Fermi energy relative to the conduction band bottom. The energy distribution of electrons in this case is described by the Fermi–Dirac statistics, i.e., all states below the Fermi level are occupied and all states above the Fermi level are vacant. In the reference frame of a moving atomic particle, the Fermi sphere is shifted and, correspondingly, the electron distribution transforms into the Doppler–Fermi–Dirac distribution, in which vacant states below the Fermi level and occupied states above it appear [29].

The kinematic effect strongly affects the resonant charge transfer, making it possible when it is energy-forbidden at low velocities. Electron exchange under grazing-incidence scattering of ions is considered in more detail in Section 3.3.1.

2.1.3.5 Neutralization of alkali metal ions. Due to the relatively small ionization energy of alkali metal atoms (5.39 eV for Li, 5.14 eV for Na), their energy position is near the Fermi level of most metals. The probability of Auger neutralization in this case is low; therefore, the neutralization of alkali metal ions is implemented at the expense of resonant electron tunneling. Since the electron energy does not change in a resonant transition, the neutralization of alkali metal ions is possible only if the level of the ion is lower than the Fermi level of the metal. We recall that, because of the interaction with image charges, the energy level of positive ion grows near a metal surface [13].

Figure 5 illustrates the process of neutralization of positive alkali metal ions. Let us denote by z_F the distance to the surface, at which the ion level crosses the Fermi level. In view of the energy, at distances $z < z_F$, only the loss of an electron by the atomic particle is possible. Therefore, near the surface, an equilibrium charge distribution forms, in which the atomic particle is a positive ion. The final charge state of the scattered atomic particle forms during the departure of the particle from the surface at distances $z > z_F$, when the resonant neutralization of a positive ion becomes possible.

Thus, the probability of neutralization increases with decreasing distance z_F. Since the efficiency of resonant transitions exponentially decreases with the distance to the surface, the final probability of alkali metal ion neutralization critically depends on the distance z_F. For example, the energy position of K (ionization energy 4.34 eV) is higher than the Fermi level in most metals. Therefore, the probability of K^+ neutralization is close to zero [30], whereas for Li ions, with an ionization energy of 5.39 eV, the neutralization begins at the distances $z_F \sim 5-10$ a.u. and is sufficiently efficient (the probability of neutralization $\sim 10-90\%$) [30].

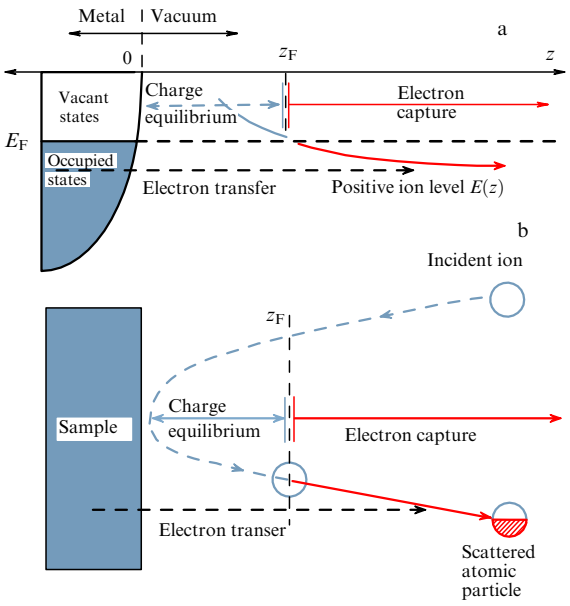

Figure 5. Illustration of the final charge state formation model by the example of alkali metal ion neutralization.

Table 1. Positive charge preservation probability under exposure of a Cu(100) surface with the work function 5.10 eV to positive alkali metal ions with the energy of 5 keV. The scattering angle is 30° [18].

Atom	Ionization energy, eV	P^+, %
Li	5.39	63.4 ± 1.5
Na	5.14	75.9 ± 0.4
K	4.34	99.4 ± 0.1

The metal work function also affects the distance z_F and the neutralization probability. For example, the neutralization probability for Na^+ (ionization energy of 5.14 eV) on the surface of Cu(110) with the work function of 4.48 eV is several times greater than that on the surface of Cu(111) with the work function of 4.94 eV [31]. A vivid example of the work function (Fermi level) effect on a resonant electronic transition is presented in Refs. [32, 33]. It was shown that, due to the change in the metal work function under an increase in the coating with Cs adsorbate, the probability of neutralization changes by an order of magnitude (see also experimental data in Section 3.5). The characteristic neutralization probability of alkali metal ions strongly depends on their energy position with respect to the metal Fermi level (Table 1).

It should be noted that, upon taking account of the overlap of the wave functions of an alkali metal atom and the surface atoms, the energy position of alkali metal ions near the surface ($z < 4$ a.u.) can turn out to be lower than the Fermi level [34]. Therefore, in the immediate vicinity of the surface, an alkali metal ion can be fully or partially neutralized. However, when moving off the surface with a small velocity (up to 0.05 a.u.), the alkali metal atom is virtually completely ionized at a distance of up to 5 a.u. from the surface, where its energy level is higher than the Fermi level of the metal [31]. Therefore, the above (simplified) model of neutralization of alkali metal ions works well for low-energy ions (up to 2 keV).

2.1.3.6 Neutralization of inert gas ions and negative ion formation. The neutralization of inert gas ions occurs via a combination of resonant electronic transitions and Auger processes. For hydrogen, the ionization energy is 13.6 eV and the corresponding energy position of the atom is close to the conduction band bottom of many metals. Therefore, in the neutralization of H^+, both resonance and Auger processes can be involved. In the case of He^+ (ionization energy 24.6 eV) and other ions with a high ionization energy, as a rule, the Auger neutralization occurs. The characteristic distance at which H^+ is neutralized is about 3 a.u. from the surface.

In many experiments reported in the literature, the yield fraction of H^- ions under the incidence of an H^+ primary beam is studied. The electron affinity energy for hydrogen (i.e., the energy difference between the states of H^0 and H^-) amounts to 0.75 eV. Due to interaction with the image charge, the energy position of H^- depends on the distance to the surface as approximately $-1/4z$. The energy level of H^- crosses the Fermi level of metals at distances of ~ 5 a.u. and approaches -0.75 eV at large distances. The H^- ion formation occurs in two stages. First, an almost 100% neutralization of H^+ occurs (see the description above). At the second stage, the final charge state of the hydrogen atom moving off the surface is formed due to competing resonant processes of electron capture by the H^0 atom and the loss of an electron by the H^- ion. At low velocities of rebound, the final charge state formation occurs at a distance of ~ 9 a.u. from the surface.

2.2 Some specific features of the experimental investigation of electron exchange

The investigation of electron exchange between atomic particles and a surface of solids implies conducting experiments under high-purity conditions. In particular, the composition and structure of the surface must be (almost) constant during the experiment, and the beams of primary/secondary particles should not encounter significant obstacles, e.g., molecules of atmospheric and residual gases. To ensure the above requirements, experiments should be carried out under the conditions of a super-high vacuum ($10^{-10}-10^{-11}$ Torr).

For correct interpretation of experimental results on electron exchange, the experiments should be carried out with 'clean' surfaces that satisfy the following criteria:

(1) There should be no impurities or adsorbates. If the experiment is aimed at the study of impurities/adsorbates, they are deposited on an initially clean surface under controlled conditions.

(2) The surface orientation along 'low-index' planes is desirable.

(3) The surface should be smooth at the atomic level (in many experiments, the smoothness criterion is the presence of no more than one step for every 1000 atomic rows).

To prepare experimental samples, additional units should be integrated in the superhigh-vacuum setup for surface cleaning, sedimentation of adsorbates or thin films/clusters, determination of surface orientation, measuring the sample work function, etc., depending on the goal of the performed experiment. Preparing experimental samples, testing their 'purity', and determining orientation using additional techniques are rather laborious processes, taking up to several months [13].

To minimize the surface destruction by an ion beam, in modern setups, small currents (0.1–100 nA) and a pulsed ion beam mode are used [14]. It is also worth noting that the experimental study of electron exchange with dielectric surfaces is complicated by the sample charging effect [14, 35].

The experimental study of electron exchange with a surface requires measuring a relative number of charged and neutral particles. Charged particles (ions) are detected using electrostatic analyzers, which are not expensive and are widely used in experimental setups. Detecting neutral atoms requires time-of-flight (TOF) analyzers. Their use is limited for the following reasons:

(1) TOF analyzers are expensive (about 150,000 USD) and bulky (1–2 m long), which hampers their use in the angular scanning mode.

(2) Detectors in TOF analyzers have various sensitivities to neutral and charged atoms, which requires a nontrivial calibration procedure [14].

Therefore, the actual situation is such that in most LEIS setups only positive ions are detected using electrostatic analyzers. For example, according to data from 2016, the serial Qtac 100 setup (IONTOF, Germany) is not equipped with a TOF analyzer [15]. The analysis of publications in the last 10 years shows that about seven research teams in the world intensely use TOF analyzers in studies of electron exchange.

2.3 Approaches to computational-theoretical study of electron exchange

The information extracted from experiment is limited and, therefore, computational modeling of electron exchange is important for understanding its fundamental regularities. For example, we can measure the probability of electron transition between an atomic particle and a surface, but we cannot determine the distribution of electrons transferred into a metal. Generally, electron exchange is described by the multielectron time-dependent Schrödinger equation

$$\mathrm{i}\,\frac{\partial\Psi(\mathbf{r}_1,\ldots,\mathbf{r}_N,t)}{\partial t}=\hat{H}(\mathbf{r}_1,\ldots,\mathbf{r}_N,t)\Psi(\mathbf{r}_1,\ldots,\mathbf{r}_N,t)\,. \quad (3)$$

The calculation of resonant charge transfer is a complex quantum mechanical problem; therefore, a number of approximations are used to solve it. The *adiabatic approximation* is often used, in which the efficiency of electron tunneling Γ is considered depending only on the distance to the surface, but the motion of the atomic particle and the phase of the wave function are not taken into account [36].

The simplest physical approach to the calculation of the charge state of a scattered atomic particle is based on integration of the semiclassical *kinetic equation* (or balance equation)

$$\frac{\mathrm{d}P}{\mathrm{d}t}=\Gamma_{\mathrm{capture}}(z)(1-P)-\Gamma_{\mathrm{loss}}(z)P\,. \quad (4)$$

Here, P is the probability of finding the atomic particle in a definite charge state (e.g., a neutral Li atom or a negative hydrogen H^- ion). The rates of electron capture $\Gamma_{\mathrm{capture}}(z)$ and loss $\Gamma_{\mathrm{loss}}(z)$ are specified empirically or calculated within the frameworks of certain models.

In the 1980s, Brako and Newns proposed a relatively rigorous formal description of resonant charge transfer — the so-called Anderson–Newns model — in which an electron transition between the states of atomic particles and a solid was considered using the perturbation theory [8]. In terms of the secondary quantization, the time-dependent Anderson–Newns Hamiltonian has the form

$$\hat{H}\big(z(t)\big)=\sum_{\mathbf{k}}E_{\mathbf{k}}n_k+E_{\mathrm{a}}\big(z(t)\big)n_{\mathrm{a}}+\sum_{\mathbf{k}}\Big(V_{\mathbf{k}}\big(z(t)\big)c_k^{+}c_{\mathrm{a}}+V_{\mathbf{k}}^{*}\big(z(t)\big)c_{\mathrm{a}}^{+}c_k\Big)\,, \quad (5)$$

where $E_{\mathbf{k}}$ are the energy levels of the electron in the solid, $E_{\mathrm{a}}(t)$ is the atomic particle electron energy, $V_{\mathbf{k}}$ are the interaction matrix elements, and $n_{\mathrm{a}}=c_{\mathrm{a}}^{+}c_{\mathrm{a}}$ and $n_k=c_k^{+}c_k$ are the populations of the atomic particle and the lattice states.

However, practical applicability of this model is restricted by the necessity to specify the interaction matrix elements, in the calculation of which essential simplifying assumptions are used, including the adiabatic approximation. It is worth noting that the nonadiabatic effects of electron exchange greatly (up to two times) affect the final charge state [37].

In recent decades, a wave packet propagation (WPP) method has been developed, which, in contrast to the two above approaches, does not rely on the adiabatic approximation [38–41]. The WPP method considers the tunneling of an active electron from the atomic particle to the metal surface through the potential barrier separating them. The metallic surface and the atomic particle are described by means of pseudopotentials, direct analogs of the effective single-electron potential in the density functional theory (detailed examples and characteristics of pseudopotentials are considered below). The time evolution of the active electron wave function $\Psi(\mathbf{r},t)$ is calculated by numerical solving the time-

dependent Schrödinger equation

$$\mathrm{i}\,\frac{\partial\Psi(\mathbf{r},t)}{\partial t}=\left[-\frac{\Delta}{2}+V_{\mathrm{atom}}(\mathbf{r})+V_{\mathrm{surface}}(\mathbf{r})\right]\Psi(\mathbf{r},t)\,. \qquad (6)$$

The ground state $\Psi_0(\mathbf{r})$ of the atomic particle active energy level is commonly taken for an initial condition. The potential relief affecting the active electron in the process of interaction of the atomic particle with the metal surface is obtained by simple superposition of pseudopotentials of the metal, V_{surface}, and the atomic particle, V_{atom}, which is an acceptable approximation if the distance between the atomic particle and the surface exceeds 3 a.u. [13].

Equation (6) describes electron tunneling through the potential barrier separating the atomic particle and the surface. Numerical solving Schrödinger equation (6) yields the dependence of the active electron wave function on coordinates and time $\Psi(\mathbf{r},t)$ and, correspondingly, the active electron distribution density $\rho(\mathbf{r},t)=\Psi^*(\mathbf{r},t)\Psi(\mathbf{r},t)$ at any moment of time. Projecting $\Psi(\mathbf{r},t)$ on the ground state of the atomic particle electron, we obtain the autocorrelation function of the system:

$$A(t)=\left\langle\Psi_0(\mathbf{r})|\Psi(\mathbf{r},t)\right\rangle, \qquad (7)$$

the square of the modulus of which gives the atomic particle population, i.e., the probability of finding the electron in its ground state:

$$P(t)=\left|A(t)\right|^2. \qquad (8)$$

To calculate the probability of electronic transition, i.e., the probability of capture or loss of the electron by the atomic particle, it is necessary to specify correctly the trajectory of the atomic particle and its initial charge state, and to determine the regions in which the loss or capture of the electron is possible.

Besides the direct modeling of the electron loss by the atomic particle, the WPP method can be applied to calculate the electron exchange efficiency (energy level width) for subsequently solving the kinetic equation. In the rough approximation, the energy position and the energy level width of the atomic particle are found assuming the ground state exponential decay

$$\left|A(t)\right|^2=\left\langle\Psi_0(\mathbf{r})|\Psi(\mathbf{r},t)\right\rangle\approx\exp\left(-\mathrm{i}Et\right)\exp\left(-\Gamma t\right), \qquad (9)$$

i.e., the energy position (in the atomic system of units) is the frequency of the autocorrelation function oscillations, and the energy level width is the damping coefficient of its modulus. More precise characteristics of the resonant transition, including the density of electron states and atomic energy level width, are obtained from the Laplace transform of the autocorrelation function $A(t)$ of the system:

$$\left|G(\omega)\right|^2\equiv\left|\int_0^\infty \mathrm{d}t\exp\left(\mathrm{i}\omega t\right)A(t)\right|^2. \qquad (10)$$

It is worth noting that, according to [39], the particular form of the wave function $\Psi_0(\mathbf{r})$ of the active electron ground state has practically no effect on the electronic transition efficiency.

Since the WPP method does not rely on the adiabatic approximation, it can be used to model 'fine' nonadiabatic effects [37], which is an important advantage of the method [42]. Another significant merit of the WPP method is the possibility of direct visualization of the electronic transition dynamics (evolution of electron density in time and space), in contrast to the Anderson–Newns model and the kinetic equation, in which only level populations are calculated.

The drawbacks of the method include the limited area of application: in its base form, the WPP method is suitable for the description of the electron transfer from an atomic particle to a metal surface. However, the WPP method was successfully applied to the description of the electron capture during the neutralization of alkali metal ions [37]. Direct modeling of the electron capture by an atomic particle is difficult, because the electron states in a metal can hardly be described by a single-electron wave function. Therefore, in the electron capture modeling, the semiempirical concept of losing an electron hole by the atomic particle is used [37]. These issues are considered in more detail in [38].

The shape and parameters of potentials that describe various atomic particles, including the negative hydrogen ion and alkali metal ions, are presented in Refs. [43, 44]. The pseudopotential for describing a metal surface is, generally, a single-electron effective potential used in the Kohn–Sham equations (density functional theory). Actually, it describes the potential relief 'seen' by the active electron in a solid. However, since dealing with 3D pseudopotentials is difficult because of numerical complexity, model one-dimensional pseudopotentials depending only on the distance from the surface became widely used [45, 46]. In addition to the potential relief inside the solid, they take into account the near-surface potential barrier, arising due to the interaction of the electron with the image charge. It should be noted that the parameters of model pseudopotentials of both types were chosen by comparing the results of calculations using the density functional theory and electron emission experiments. The pseudopotentials for different types of metal surfaces are described in more detail in Sections 3.1 and 3.2.

Because of the numerical complexity of the direct solution of the 3D time-dependent Schrödinger equation, approximate one- and two-dimensional approaches were used until recently, considering the problem in the approximation of spherical or cylindrical symmetry, respectively. However, recently, a three-dimensional version of the WPP method was implemented using 3D potentials that describe a metallic surface at the atomic level [47–49].

3. General regularities of resonant charge transfer

In studies of electron exchange between atomic particles and a metal surface, the formation or decay of a negative hydrogen ion is often considered a benchmark problem. This is due both to the relatively simple theoretical description of the H^- ion (see the analytical potential in [44]) and to the fact that the probability of H^- ion formation substantially depends on the surface properties and scattering parameters. For example, in the problem of H^+ neutralization on a metal surface, which is 'simpler' from a theoretical point of view, the neutralization probability approaches 100%, so that this problem is not suitable for revealing the factors affecting the electron exchange. It should be noted that the regularities of forming a number of other negative ions (O^-, S^-, F^-, Cl^-, etc.) agree with those of H^- formation [36].

The main factors affecting the probability of charge transfer (electronic transition) are the surface properties and the velocity of the scattered particle moving from the surface [50–53]. For a fixed scattering angle, the velocity of the atomic particle departure is determined by the energy of the primary beam. The normal component of the velocity determines the duration of interaction with the surface and, therefore, affects the electron exchange. The parallel component of the velocity greatly affects the electron exchange in the case of grazing-incidence scattering of ions because of the kinematic effect (see Section 2.1.3.4). The zenith angle of scattered particles relative to the surface affects the electronic exchange mainly because of a change to the normal velocity component and, consequently, the duration of particle–surface interaction.The azimuthal direction of the beam motion, i.e., the influence of the crystal structure of the surface, is most obviously manifested in the case of grazing-incidence scattering. The incidence angle of low-energy ions has no substantial effect on the electron exchange with metal surfaces due to the effect of memory loss of the initial charge state (see Section 2.1.3.3).

Section 3 focuses on the interpretation and computational-theoretical description of experimental data on the neutralization of alkali metal ions and the formation/decay of negative ions. The first theoretical papers were devoted to considering electron exchange with metals described by the free-electron model (see Section 3.1). In Section 3.2, we consider the electron exchange taking into account the realistic electronic structure and nonadiabatic effects. Section 3.3 investigates the effect of ion beam energy (velocity of atomic particles) on the electron transfer probability and the related parallel velocity effect. The electron exchange with surfaces containing nanosystems, defects, and adsorbed atoms is considered in Sections 3.4.and 3.5.

3.1 General regularities of electron exchange with metals in the free-electron model

A number of important phenomena in metals are explained by the free-electron model. Within the framework of this model, positively charged ion cores of the metal are assumed to be efficiently shielded by the valence electrons, so that the electrons are affected by a constant potential independent of the crystal structure of the metal. Conduction electrons are considered an ideal Fermi gas, and their wave functions are described by plane waves. The band structure in this case corresponds to the parabolic dispersion law. In the wave vector space, all occupied electronic states are within the so-called Fermi sphere ($k_F = \sqrt{2E_F}$).

A metal surface in the free-electron model can be described using the Jennings potential [45], incorporating a potential well with a plane bottom inside the metal and a potential barrier accounting for the interaction of electrons with the image charge in a vacuum:

$$V_J(z) = \begin{cases} \dfrac{1-\exp(\lambda z)}{4z}, & z < 0, \\ \dfrac{-U_0}{1+A\exp(-Bz)}, & z \geqslant 0, \end{cases} \qquad (11)$$

where $B = U_0/A$; $A = -1 + 2U_0/\lambda$; and the values of parameters U_0 and λ for a number of surfaces, including Al(100), Ni(100), Cu(110), Ag(110), W(100), and W(110), are summarized in Ref. [45]. The Jennings potential depends only on the distance to the surface.

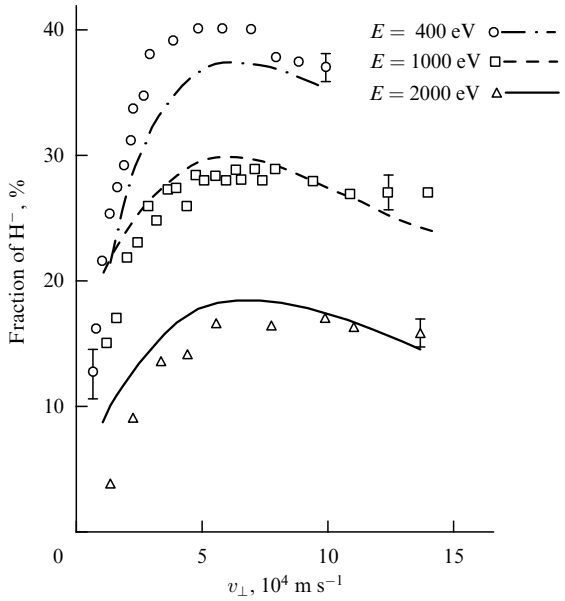

Figure 6. Probability of H^- ion formation as a function of the normal velocity of ion departure from a W(110) surface coated with Cs adsorbate [54]. The symbols represent the experimental data and the solid lines show the results of calculations using the Anderson–Newns model.

The free-electron model implies the free motion of electrons inside the metal in all directions. Therefore, in the process of transfer from an atomic particle to the metal, the electron tunnels along the normal to the surface and propagates infinitely into the metal. The possibility of backward tunneling of the electron is practically absent in this case. The atomic particle population is described by a descending exponential function of time.

In metals described by the free-electron model, as a rule, the adiabatic approximation is valid at low energies (up to a few keV) of atomic particles. The electron transfer efficiency $\Gamma(z)$ exponentially decreases with distance from the surface. The probability of electronic transition can be calculated using the kinetic equation (see Section 2.3). The Anderson–Newns model also gives good results in the case of electron exchange with surfaces described by the free-electron model. Figure 6 shows the probability of formation of H^- ions depending on the normal velocity of atomic particle departure from the W(110) surface coated with Cs adsorbate. The nonmonotonic behavior of the dependence is explained in original paper [54] as a consequence of the kinematic effect (see Section 2.1.3.4). It is worth noting that in this paper the energy position of the H^- ion was an approximation parameter rather than being calculated *ab initio*.

3.2 Taking into account the realistic electronic structure and nonadiabatic effects of electron exchange

The idealized free-electron model is quite applicable to some metals, e.g., aluminum. However, for many other metallic surfaces, it is necessary to account for their real electronic structure [25]. Due to the 3D crystal structure of real metals, there can be bands where the motion of electrons in some directions is forbidden in a certain range of energies. Note that an electron can move in other directions, so that such bands are not traditional ('completely forbidden') band gaps. In the case of metal surfaces with restricted motion of electrons along the normal, the term *projected band gap* is

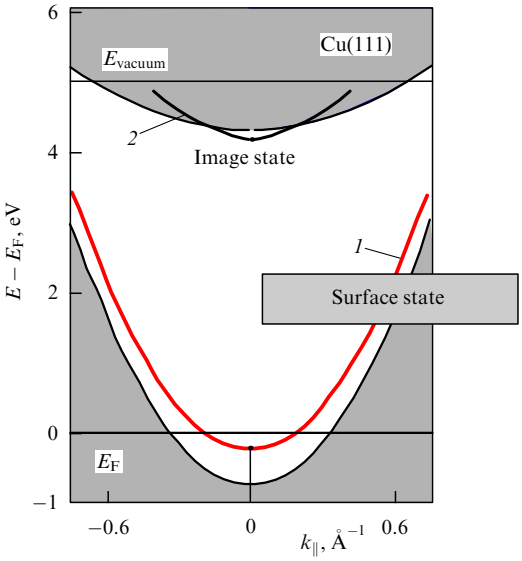

Figure 7. Electronic structure of a Cu(111) surface. The allowed electron energy is presented as a function of the wave vector component parallel to the surface. The grey region corresponds to allowed states, the red line (*1*) shows the surface state, the black line (*2*) shows the image state.

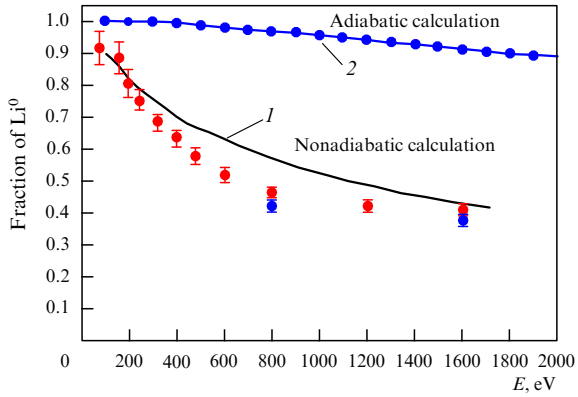

Figure 8. Comparison of the experimental and calculated dependences of Li^+ neutralization probability on the primary beam energy during the departure from an Ag(100) surface [37]. The incidence angle of the primary Li^+ beam is 45° to the surface. The spectrum of the scattered Li atoms (Li^+/Li^0) is measured along the normal to the surface. Solid black line (*1*) shows the result of 'nonadiabatic' calculations using the WPP method. Blue line (*2*) with dots shows the results of 'adiabatic' calculations using the kinetic equation.

used. The motion of an electron along the normal is restricted for the surfaces (100) and (111) in a numbers of metals, e.g., Ag, Cu, and Au.

Figure 7 shows the electronic structure of a Cu(111) surface near the Brillouin zone center ($k_z = 0$, $k_\parallel = 0$). In this case, the electron motion along the normal to the surface is restricted in the range of energy from −0.7 to −5.8 eV relative to the vacuum level. For surfaces with restricted electron motion, real (nondegenerate) surface states and image electron states can exist [46]. The surface and image states are localized in the near-surface region. On the one hand, the electron cannot 'penetrate' into the bulk metal due to the restriction of normal propagation and, on the other hand, the electron cannot move off the surface to the vacuum zone because of the attractive potential of the image charge.

To describe metal surfaces with a restricted motion of electrons, a one-dimensional periodic potential proposed in [46] is often used. The potential is expressed as follows:

$$
\begin{aligned}
V_1(z) &= A_{10} + A_1 \cos\left(\frac{2\pi z}{a_s}\right), && z \leqslant 0, \\
V_2(z) &= -A_{20} + A_2 \cos\left(\beta(z)\right), && 0 < z \leqslant z_1, \\
V_3(z) &= A_3 \exp\left(-\alpha(z - z_{im})\right), && z_1 < z \leqslant z_{im}, \\
V_4(z) &= \frac{\exp\left[-\lambda(z - z_{im})\right] - 1}{4(z - z_{im})}, && z_{im} < z,
\end{aligned}
\qquad (12)
$$

where parameters a_s, A_{10}, A_1, A_2, and β are determined by comparison with experimental data, and the rest of the parameters are found from the continuity condition for the potential and its first derivative [46]. The above potential accounts for the realistic electronic structure of metals and correctly describes the energy and localization of imaginary and surface charges. In original paper [46], examples of pseudopotential parameters are presented for Cu(100), Cu(111), Ag(100), Ag(111), Au(100), Au(111), Al(111), Li(110), Na(110), Be(0001), and Mg(0001) surfaces.

The restriction of electron motion along the normal to the surface considerably affects the charge transfer, since the normal direction is preferable for electron tunneling between the atomic particle and the metal. When considering a transfer of an electron from the atomic particle to the metal, the electron initially tunnels along the normal to the surface, but is 'reflected' from the periodic quasipotential and has to propagate mainly parallel to the surface, i.e., the electron occupies the allowed states with sufficiently large values of $k_\parallel$. For example, an electron occupying the Cu(111) Fermi level should have $k_\parallel$ of not less than 0.15 a.u. (0.3 Å^{-1}). In this case, surface and image electronic states are also populated and significantly involved in the charge transfer; this issue is thoroughly considered in Ref. [42].

For most surfaces with restricted motion of electrons, the adiabatic approximation is not applicable or leads to considerable errors. Nonadiabatic electron transfer effects are considered in [37] using the example of neutralization of Li^+ ions on the Ag(100) surface with restricted electron motion along the normal to the surface. The authors of [37] compared the results of 'adiabatic' calculations using the kinetic equation and direct calculations using the WPP method considering the nonadiabatic effect. From Fig. 8, it is seen that the results of calculations in the adiabatic approximation differ by a factor of 2 from those of experiment, while the dynamical calculations by the WPP method taking into account the realistic metal electronic structure quantitatively describe the experimental data.

Like the WPP method, the Anderson–Newns model can consider the realistic electronic structure of a metal. For example, relatively new paper [55] reports the calculations of electron exchange taking into account the metal three-dimensional crystal structure. The presented calculations demonstrate the dependence of the electronic transition probability upon the azimuthal direction of atomic particle motion. However, no comparison was carried out with appropriate experiments, in which the orientational (azimuthal) dependence of electron exchange manifested itself (see, e.g., Ref. [6] and Section 3.3.1). Since in the calculation of interaction matrix elements in the Anderson–Newns model the adiabatic approximation is used, this model is not suited

for considering nonadiabatic effects of electron exchange (see some examples in Section 3.3.2).

3.3 Effect of atomic particle velocity on electron exchange

The scattering of ions can be conventionally divided into scattering at normal angles (the incidence/reflection angle is greater than 30° relative to the surface) and grazing-incidence scattering (the incidence/reflection angle is smaller than 30° relative to the surface). The electron exchange in these cases is commonly considered separately because of different electron exchange effects manifesting themselves in them.

In the case of grazing-incidence scattering (see Section 3.3.1), the adiabatic approximation is applicable, since the normal component of the atomic particle velocity amounts to about 0.01 a.u. For normal-angle scattering (see Section 3.3.2), nonadiabatic effects of electron exchange can manifest themselves.

3.3.1 Grazing-incidence scattering. A typical problem is the formation of a negative hydrogen ion under the scattering of the primary H^+ beam at grazing angles. Let us recall that the neutralization of the primary H^+ beam occurs due to resonant and Auger processes in the immediate vicinity of the surface with a probability close to 100%. Then, the formation of an H^- ion is caused by competing resonant processes of electron loss and capture. During grazing-incidence scattering of atomic particles, an essential role in the exchange of electrons is played by the kinematic effect (see Section 2.1.3.4) or the parallel velocity effect [6, 36, 56, 57].

A general feature of grazing-incidence scattering is the bell-shaped or monotonically decreasing dependence of the electronic transition probability on the parallel component of ion velocity (Fig. 9). The form of this dependence is explained well by the model of intersecting Fermi spheres of the metal and the transferred electron, in which the transition probability is proportional to the intersection area. With the transformation of electron distribution in the k-space from the moving reference frame of the ion to the fixed reference frame of the surface taken into account, a relative shift of the spheres by the magnitude of the ion motion velocity appears. Therefore, the area of intersection of two spheres depends on the magnitude of the ion parallel velocity. Then, the bell-shaped dependence of the H^- formation probability is easily explained using geometric reasons.

In an experimental study carried out in 2000 [36], the authors detected the dependence of formation probability on the azimuthal angle in the grazing-angle scattering of H^- by a Cu(110) surface. For Cu(111), no such dependence was found. To explain this effect, in the model of intersecting Fermi spheres, the anisotropy of electron propagation on the Cu(110) surface was taken into account [38]. Due to the anisotropy, the active electron distribution in the k-space has the form of an ellipsoid rather than a sphere. Therefore, the area of intersection of the ellipsoid and the sphere depends not only on the magnitude of parallel velocity, but also on the azimuthal direction of the atomic particle motion (Fig. 10).

Considering the electron propagation anisotropy allowed a quantitative description of experimental data on the dependence of H^- ion formation probability upon the azimuthal angle upon grazing-incidence scattering from the Cu(110) surface (Fig. 11).

3.3.2 Normal-angle scattering. Let us consider the influence of atomic particle velocity (energy) in the case of normal-angle scattering via the example of neutralization of alkali metal positive ions. An example of the experimental dependence of neutralization probability on the energy of an outgoing atomic particle is presented in Fig. 8. The neutralization probability is seen to decrease with the growth of energy (velocity) of the outgoing atomic particle. The descending dependence is logically explained by the fact that at low velocities of moving off the time of interaction with the surface is longer, so that the probability of capturing the electron by a positive ion increases.

However, in Ref. [52], an interesting experimental effect was revealed. In contrast to Ag(100) and Ag(111) surfaces,

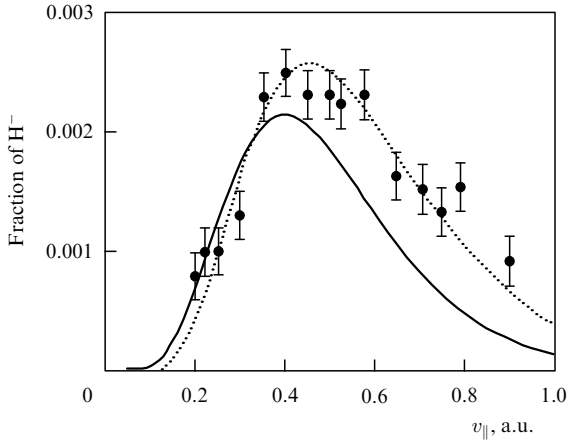

Figure 9. Comparison of the experimental and calculated H^- ion formation probability during scattering on an AL(111) surface depending on the ion beam velocity component parallel to the surface [6].

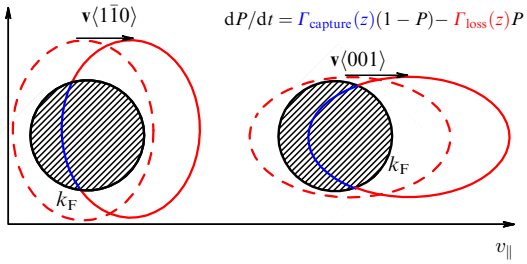

Figure 10. (Color online.) Intersection of the Fermi sphere of a metal with the ellipsoid of active electron detection probability distribution.

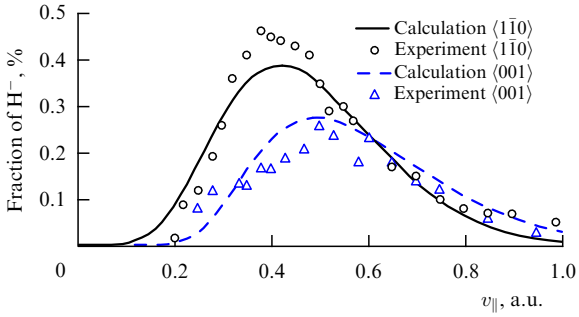

Figure 11. Comparison of the calculated results [38] with the experimental data [6, 13, 36]. Shown is the fraction of H^- ions scattered from a Cu(110) surface as a function of the ion beam velocity component parallel to the surface. The normal component of the primary beam velocity of H^+ is 0.02 a.u.

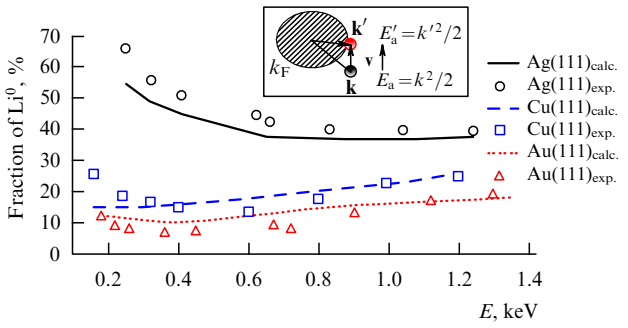

Figure 12. Calculated [38] and experimental [52] Li^0 yield fraction as a function of the primary beam energy for different surfaces (see legend). The incidence angle of the Li^+ primary beam is 45° to the surface. The spectrum of the scattered Li (Li^+/Li^0) atoms is measured along the normal to the surface. The inset illustrates the improved physical model of the final charge state formation: k_F is the metal Fermi sphere, $\mathbf{k}$ and E_a are the wave vector and energy of the active electron considered statically, and $\mathbf{k}'$ and E'_a are the wave vector and energy of the active electron with the atomic particle motion taken into account (see comments in the text).

the yield fraction of Li^0 under electron exchange with the Cu(111) and Au(111) surfaces nonmonotonically depends on the beam energy (Fig. 12). Note that the scattered particles were detected along the normal to the surface; therefore, the results are not related to the parallel velocity effect. The original paper presented only the calculation results for an Ag surface with free electron motion, and the question of nonmonotonic energy dependence of the Li^0 yield fraction remained open.

In later papers of 2017 and 2012, the dependence of alkali metal ion neutralization probability on the energy of an outgoing particle was studied using the Anderson–Newns model [31, 58]. To calculate the interaction matrix elements in the first case, the density functional theory was applied. In the second case, the authors used the method of linear combinations of atomic orbitals (LCAOs). In Ref. [31], the results considerably differ from the experimental data, although in some cases a qualitative agreement between calculated and experimental dependences is observed. On the whole, the presented calculations do not explain the nonmonotonic behavior of the energy dependence of neutralization probability. The results of calculations in [58] demonstrate semiquantitative agreement with experimental data for the normal component of the outgoing particle energy of the order of 1 keV. However, the presented model can explain the high probability ($> 70\%$) of positive ion neutralization at small outgoing particle energies (~ 200 eV).

Nonmonotonic energy dependence of the alkali metal ion neutralization probability was explained in [38] by the difference in energy among the Fermi levels for the considered surfaces and by the differences among the dependences of z_F on the atomic particle velocity (see the model of alkali metal ion neutralization in Section 2.1.3.5). In the static case, for the Ag surface ($E_F = -4.5$ eV), z_F amounts to about 7 a.u. In the case of Cu(111) and Au(111), the distance of the intersection with the Fermi level is of the order of 8–10 a.u., because the Fermi level for these metals is lower (−4.94 eV and −5.1 eV, respectively). For a moving atomic particle, the correction to the energy position

$$\Delta E_a(z) = \frac{|k'|^2}{2} - \frac{|k|^2}{2} = \frac{|v|^2}{2} - \mathbf{vk}$$

should be taken into account. This leads to the dependence of z_F on the atomic particle velocity. The absolute value of the energy position shift for the experimentally available range of beam energies amounts to 0.05–0.2 eV and weakly depends on the target material. However, near the crossing point z_F, the dependence $E(z)$ changes faster for Ag(100)/Ag(111) surfaces than for Cu(111) and Au(111) surfaces. Therefore, to compensate the same shift of energy position in the case of Ag(100)/Ag(111) surfaces, a smaller variation of z_F is necessary. In the presented calculations, the range of z_F variation was 5.8–6.2 a.u. for Ag(100), 6.5–7.0 a.u. for Ag(111), 7.7–8.4 a.u. for Cu(111), and 7.8–9.1 a.u. for Au(111).

In accordance with the above, a qualitative explanation of the nonmonotonic energy dependence of Li^0 yield fraction consists of the balance between the influence of the interaction time (decreases with growing energy) and the averaged efficiency of electron exchange (increases with the energy because of a decrease in z_F). For low energies of Li, the changes in z_F are not large, and the probability of Li^+ neutralization is determined by the interaction time. For higher Li energies, the values of z_F substantially decrease (by a value of up to 1 a.u.), which leads to the increase in the electronic transition efficiency and the Li^+ neutralization probability.

3.4 Electron exchange with nanosystems

In the above sections, we considered the electron exchange with bulk (semi-infinite) samples in the free-electron approximation and with the realistic electronic structure of metal taken into account. Restricting the metallic sample dimensions also affects its electronic structure: the electron energy is quantized and the spatial distribution of electron density becomes discrete (see scanning tunneling microscopy (STM) images in Fig. 13 [59]). An electron in a nanosystem is described by a set of discrete eigenstates, which it can occupy, rather than by plane waves. Correspondingly, the restriction of sample dimensions will affect the electron exchange with atomic particles [60–66]. From the point of view of fundamental science, the quantum behavior of nanostructures is promising for developing various new technologies, e.g., single-electron transistors or molecular computers [67, 68]. Concerning practical application, nano-

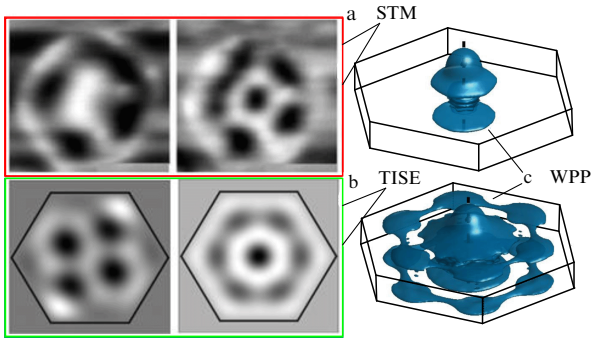

Figure 13. Illustration of the discrete electronic structure of nanosystems. (a) STM images of electron density for some eigenstates on the surface of a hexagonal Ag nanocluster with an inner diameter of 10.4 nm [59]; (b) electron density calculated using the time-independent Schrödinger equation (TISE); (c) results of WPP modeling of the electron funneling from an H^- ion to a nanocluster after 300 and 600 atomic units of time from the beginning of interaction.

structures are already used as gas sensors [69–72] and catalysts [73] (see Section 4.3.1).

The theoretical study of electron exchange with nanosystems began by considering electron exchange with thin metallic films [74]. Qualitatively, the electron exchange with nanosystems is analogous to the case of surfaces with restricted electron motion: the electron density distribution is discrete and the electron propagates mainly parallel to the surface (Fig. 13c). Figure 13 shows the discrete distribution of electron density in an Ag cluster. It is seen that the results of calculations (Figs 13b, c [75]) are in good agreement with the data obtained by STM (Fig. 13a).

While in the electron exchange with a bulk sample, the main factor determining the efficiency is the distance between the atomic particle and the surface; in the case of a nanosystem, the electron exchange efficiency is also highly dependent (up to an order of magnitude) on the nanosystem dimensions and the lateral position of the atomic particle. The key point is that the efficiency of electron transfer depends on the fulfillment of resonance conditions. The maximal electron transfer efficiency is demonstrated when the energy position of the atomic particle corresponds to one of the discrete energy levels of the nanosystem. In turn, the set of electron discrete energy levels in a nanosystem depends on its dimensions.

In Ref. [60], a model problem of electron transfer between a spatially fixed ion and thin films of various thicknesses was considered. It was shown that the energy level width is a nonmonotonic function of the film thickness (the quantum-dimensional effect of electron exchange with an infinitely thin film, Fig. 14). The authors of Ref. [76] investigated electron exchange with a cluster of atoms and demonstrated the dependence of electron exchange efficiency on the ion lateral position relative to the cluster. References [62, 66] showed the quantum-dimensional effect manifestations upon varying the radius of an island thin film. It was also shown that the quantum-dimensional effect manifests itself for a radial size of the island thin film of not greater than 100 a.u. At greater sizes, the separation between the adjacent energy levels becomes smaller than the broadening of an energy level of the atomic particle, and the character of electron exchange corresponds to the interaction with a bulk sample.

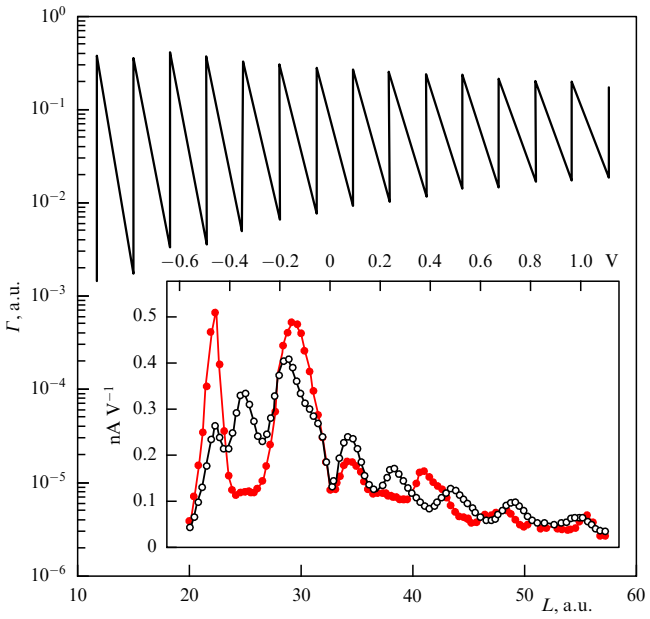

Figure 14. Electron tunneling efficiency versus film thickness [60]. The tunneling efficiency (energy level width) was calculated for the active electron of the H^- ion, located at a distance of 8 a.u. from the Al film surface. The inset shows the experimental dependences of the differential conductivity on the bias voltage for two different lateral positions of the microscope tip [79].

When solving a dynamical problem of an electron incident on the surface, it is necessary to consider the minimal time required for the manifestation of the quantum-dimensional effect. The characteristic order of magnitude for the minimal interaction time amounts to 500 a.u., which corresponds to a maximal velocity of ions of the order of 0.05 a.u. (or an energy of $\sim$ 60 eV for hydrogen ions and 2.5 keV for argon ions).

Note that the observation of effects related to the discrete electronic structure of nanosystems is difficult (unlikely) in experiments on electron exchange with atomic particles, because, in the process of atomic particle motion, the electron exchange occurs with several energy levels, thus 'averaging' the discreteness of the electronic structure. Scanning tunneling microscopy is widely used to study the electronic structure of metallic nanoclusters [77, 78]. In the STM mode, for a fixed position of the microscope tip, the dependence of differential conductivity dI/dV on the bias voltage demonstrates clearly expressed maxima, corresponding to the discrete density of electronic states in the nanocluster [79] (see the inset in Fig. 14). The cause of oscillations of both the differential conductivity and the electron exchange efficiency is the discrete electronic structure of nanosystems.

3.5 Electron exchange with surfaces comprising defects or adsorbates

The study of surfaces coated with adsorbates or comprising defects (surface reconstruction, steps, etc.) is interesting, because electron exchange essentially depends on the structure and electronic properties of the surface.

The effect of adsorbates is usually considered at the microscopic and macroscopic levels [80]. At the microscopic level, an adsorbate atom changes the local electrostatic potential in its vicinity. Therefore, the probability of electronic transition will depend on the location of atomic particle incidence on the surface [81, 82].

At the macroscopic level, the coating of the surface with an adsorbate can lead to an essential change in the metal work function, which considerably increases the probability of electron capture by the atomic particle. Figure 15 shows that the probability of Li^+ neutralization on the W(110) surface changes from 0 to 100%, with the work function changing from 5.25 to 3.5 eV due to the coating of the surface with Cs atoms. Theoretically, the measurement of neutralization probability can be used to determine the metal work function; however, no relevant publications are known by the author. This is possibly due to a substantial error ($\sim$ 0.2 eV) and the complexity of measuring the neutralization probability.[1] In Ref. [83], it was proposed to determine the work function from the position of the maximum in the dependence of neutralization probability on the parallel velocity in the case of grazing-incidence scattering of ions (see examples in Section 3.3.1), which potentially increases the measurement accuracy to 0.05 eV.

[1] The measurement of the ratio of neutral atoms to positive ions requires using time-of-flight analyzers.

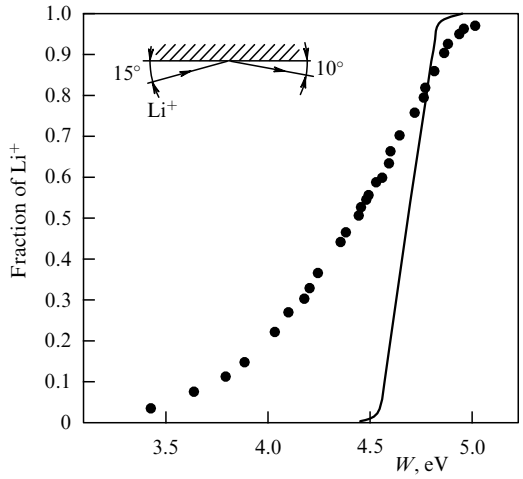

Figure 15. Li^+ fraction as a function of the electron work function (depending on the degree of coating of the W(110) surface with Cs atoms) [33].

Some authors modeled the effect of surface defects on the electron exchange [84, 85]. The influence of ion trajectories with respect to atomic steps, as well as Si surface reconstruction, was studied. However, conducting the appropriate experiments is difficult because of the complexity of preparing a surface with the specified parameters and regularity of defects.

4. Practical application of electron transfer in the process of low-energy ion scattering

In applications, the electron transfer between atomic particles and surfaces is mainly used to diagnose the surface elemental composition [14] and create high-efficiency sources of negative ions [13, 86].

In the case of electron exchange with dielectric surfaces, a considerable probability of negative ion formation (up to 100%) is observed. Therefore, this process is of practical interest for creating efficient sources of negative ions. Electron exchange can also be used to generate excited atoms, and for the capturing of and emission from spin-polarized electrons (see review [13]).

One of the most important applications of electron exchange is the quantitative diagnostics of the surface elemental composition and crystal structure of solids by means of low-energy ion scattering (see Section 4.1). In Section 4.1.3, we present examples demonstrating that ignoring electron exchange can lead to multiple errors in determining the surface chemical composition. In Section 4.1.4, recommendations are presented on improving the accuracy of chemical composition measurements by taking into account or calculating the neutralization probability. The LEIS method possesses the best surface sensitivity; it allows determining the composition of the uppermost surface layer [14, 15] (see Section 4.2). Section 4.3 considers examples of the practical application of the LEIS method.

4.1 Analysis of crystal structure and composition of a surface by the low-energy ion scattering method

4.1.1 Analysis of surface elemental composition. For the quantitative analysis of surface chemical composition by LEIS, a method of reference samples has been developed. The determination of the surface concentration of atoms is described in detail in Ref. [14]. The yield of ions scattered from a specified type of surface atom (S_i) is proportional to the concentration of this element N_i:

$$S_i = I_p t \xi R \eta_i N_i \,, \tag{13}$$

where I_p is the primary beam current, t is the signal accumulation time, ξ is the instrumental factor, including the detector collection angle, detector sensitivity, and analyzer transmission coefficient, R is an empirical factor allowing for surface roughness, and η_i is the elemental sensitivity calculated as

$$\eta_i = P_i^+ \frac{\mathrm{d}\sigma_i}{\mathrm{d}\Omega} \,,$$

with the ion yield probability P_i^+ and differential cross section of scattering $\mathrm{d}\sigma_i/\mathrm{d}\Omega$.

Knowing the experimental values of ion yield S_i, the relative surface element concentrations n_i can be determined as follows:

$$n_i = \frac{N_i}{\sum_j N_j} = \frac{S_i/\eta_i}{\sum_j S_j/\eta_j} \,. \tag{14}$$

Note that most factors in Eqn (13) (I_p, t, ξ, R) cancel, since they do not depend on the type of atom on which scattering occurs.

For a two-component surface comprising elements A and B, expression (14) is reduced to the form

$$n_A = \frac{1}{1 + \eta_{A/B} S_B / S_A} \tag{15}$$

with relative elemental sensitivity $\eta_{A/B} = \eta_A/\eta_B$.

The signal of the scattered ions S_i is found from experiment, so that, to determine the relative surface concentration of elements n_i by means of expressions (14) or (15), it is necessary to know the elemental sensitivity. To find it, the method of reference samples is used. Its essence consists of calibrating the relative elemental sensitivity $\eta_{A/B}$ with reference samples — pure substances or materials with known elemental composition. Due to the similarity of experimental conditions in the measurements of reference and studied samples, it is believed that the method of reference samples accounts for different scattering cross sections and neutralization on different chemical elements. The relative elemental sensitivity is found from expression (13) as

$$\eta_{A/B} = \frac{\eta_A}{\eta_B} = \frac{I_p t \xi R N_B / S_B}{I_p t \xi R N_A / S_A} = \frac{N_B/S_B}{N_A/S_A} \,. \tag{16}$$

The sensitivity of the LEIS method, i.e., the minimal detectable surface concentration of an element, depends on the mass ratio of the incident ions and the element under study; typical values of the sensitivity lie in the range from 0.01 to 1% [15]. The relative accuracy of the surface composition measurement by the LEIS method amounts to about 10%. LEIS belongs to surface-nondestructive methods of study, because during the spectra recording on up-to-date setups less than 0.5% of the surface atomic monolayer is sputtered [87].

4.1.2 Analysis of crystal structure by the LEIS method. Let us illustrate the analysis of crystal structure via the example of the $Cu_3Pt(111)$ surface from [88]. The analysis is based on the shadowing effect, giving rise to minima in the angular dependence of the ion yield. Note that in most LEIS experiments the direction (vector) of incidence of the primary beam and the direction of detection of scattered ions lie in one plane perpendicular to the surface. Experiments are performed either in the mode of azimuthal scanning (the sample rotates around the axis normal to the surface) or in the mode of angular scanning, in which the zenith angle of incident or detected ions relative to the surface is varied.

Figure 16 illustrates the results of zenith angle scanning of the incident beam of Li^+ ions to be scattered on a $Cu_3Pt(111)$ surface. The observed minima in the yield of scattered ions correspond to the direction of beam incidence along one of the crystal lattice directions, when the atoms of the uppermost layer shadow those of lower-lying layers. The circles mark critical angles at which the atoms of the second, third, etc., layers move out of the shadow. Note that, knowing the critical angles and having calculated the shadow cone radius, one can evaluate the change in distance between the near-surface atomic layers (surface relaxation value). Comparing the experimental angular spectra (critical shadowing angles) with the calculation results for the model crystal structure, the authors of [89] concluded that in the $Cu_3Pt(111)$ uppermost layer the Cu and Pt atoms are in one plane with an accuracy of up to 0.05 Å.

In Ref. [90], the importance of electron exchange in the crystal structure analysis was shown. It was demonstrated that the yield of neutral scattered atoms exceeds the yield of positive ions by an order of magnitude; moreover, the spectrum of neutral atoms contains information on the crystal structure, which is 'erased' if only positive ions are detected.

4.1.3 Role of electron exchange in the LEIS method. Generally, the analysis of surface composition and structure by the LEIS method requires solving the inverse problem [91]. It is necessary to construct a model of the crystal structure and choose the concentration of elements that provides the required angular and energy spectra of the scattered ions. Quantitative diagnosing requires knowledge (measured or calculated) of the scattering cross section and neutralization probability for ions [14, 92]. The first problem is fairly well studied theoretically, the elaborated pair potentials providing a good description of experimental data on scattering cross sections [93–95], whereas the electron exchange is less studied and quantitative calculation models exist only for relatively simple systems (see Section 3 and Refs. [8, 13, 18, 54]).

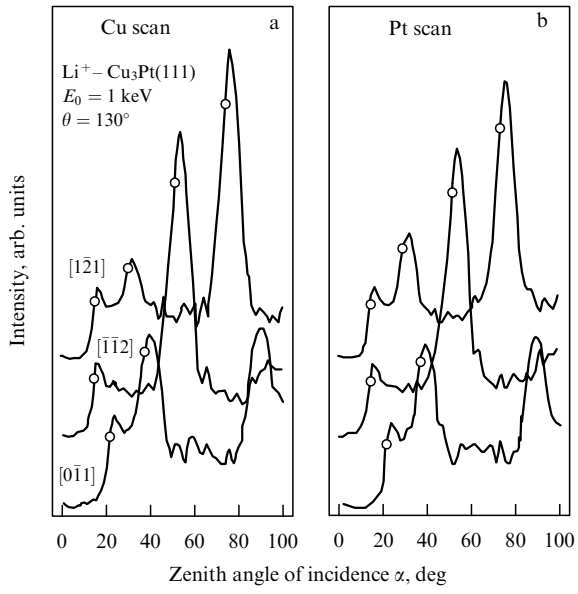

Figure 16. Yield of Li^+ ions scattered from a $Cu_3Pt(111)$ surface depending on the primary beam incidence angle relative to the surface [88]. The data are plotted for several azimuthal directions.

Note that the importance of neutralization in analyses using the LEIS method has been known for a long time. For example, the probability of neutralization of Li^+ ions in the process of scattering on Ag(100) changes by almost an order of magnitude when there is a change in the outgoing ion energy from 0.2 to 1.2 keV [37]. Therefore, correctly considering electron exchange is of key importance for a quantitative analysis. In principle, it is possible not to account for the electron exchange in the analysis of surface composition by the LEIS method if the total charge composition of the scattered particles is registered including both ions and neutral atoms. For this purpose, time-of-flight analyzers are exploited [14]; however, their use is limited due to a number of reasons (see Section 2.2).

As a specific example demonstrating the importance of taking electron exchange into account, let us consider two experiments in which the concentration of Cu and Zn in the process of their sputtering on a Pt(111) surface was measured [96, 97]. The measurements were performed by scattering Na^+ ions with an energy of 1 keV. For a better comparison of calculated results with the original data, expression (15) for the surface concentration is reduced to the form

$$N_A = \frac{1}{1 + (S_B/S_A)(1/\eta_{B/A})} . \qquad (17)$$

Since the ionization energy of Na amounts to 5.14 eV, the probability of Na^+ neutralization on the Cu/Pt(111) surface under study and the reference sample of Pt(111) is close to zero, because the Fermi level for these surfaces is substantially lower than the energy level of Na. At the same time, the work function for the reference sample of Cu(111) equals 4.94 eV, so that the neutralization probability is of the order of 10% [31]. Therefore, the elemental sensitivity to copper measured on the reference sample of Cu(111) should be corrected by division by a factor of 0.9. This is equivalent to multiplying the relative elemental sensitivity $\eta_{Pt/Cu}$ by a factor of 0.9. Correspondingly, the value of 0.07 for the surface concentration of Cu obtained in the original paper [96] will decrease to 0.063. Note that this change is inessential and lies within the experimental error. The results of calculations are presented in Table 2.

Table 2. Experimental data and results of analysis of the composition of Cu/Pt(111) and Zn/Pt(111) surfaces. The left-hand columns show experimental data and results of measurements from original papers [96, 97]. The right-hand columns present the data related to calculated element concentrations with the Na^+ ion neutralization on reference samples taken into account.

Experiment				Correction for neutralization		
A/B	S_B/S_A	$\eta_{B/A}$	N_A	P^+	$\eta_{B/A}$	N_A
Cu/Pt	14.88	1.12	0.07	0.9	1.008	0.063
Zn/Pt	64.6	3.4	0.05	0.4	1.19	0.018

A much more noticeable effect of neutralization manifests itself in the case of a Zn/Pt(111) bimetallic surface. Since the Fermi level of the surface under study and the reference sample of Pt(111) is significantly lower than the Na energy level, the probability of Na^+ neutralization on these surfaces is inessential. However, for the reference surface of Zn, the work function is about 4.4 eV and, therefore, the Na^+ neutralization will begin at smaller distances and occur much more efficiently (see Section 2.1.3.5). According to the experimental data in [31], the probability of Na^+ neutralization on the Cu(110) surface with a similar work function is estimated as 60–70%. Therefore, the relative elemental sensitivity $\eta_{Pt/Zn}$ should be multiplied by a factor of 0.4. This leads to a threefold (!) correction of the surface Zn concentration (see Table 2).

The manifestation of the Na^+ neutralization effect also becomes obvious from an analysis of relative elemental sensitivity values $\eta_{Pt/Cu}$ and $\eta_{Pt/Zn}$ in Refs. [96, 97]. It should be clarified that these two experiments were carried out by the same research team under the same experimental conditions (beam energy, incidence angle, etc.). However, the relative elemental sensitivities differ greatly: $\eta_{Pt/Cu} = 1.12$, $\eta_{Pt/Zn} = 3.14$. Since Cu and Zn are neighboring elements in the periodic table, they have close values of nucleus mass and charge. Therefore, it seems impossible to explain the above significant difference by different scattering cross sections. With the ion neutralization taken into account, the values of $\eta_{Pt/Cu}$ and $\eta_{Pt/Zn}$ become commensurable (see Table 2).

4.1.4 Improving the quantitative analysis accuracy of the surface composition by means of scattering of low-energy alkali metal ions. In the present section, we consider the possibility of increasing the accuracy of surface elemental composition analysis by considering ion neutralization in the LEIS method. We recall that the commonly accepted approach to measuring surface concentration by LEIS is based on measuring the relative elemental sensitivity on reference samples (see Section 4.1.3). If all scattered atomic particles are registered, both neutral and positively charged, then the neutralization effect should not be taken into account. However, due to the relative expensiveness of time-of-flight analyzers and the complexity of their calibration, in most experimental setups only positive ions are detected using electrostatic analyzers.

The neutralization effect may be disregarded if the energy level of the ion is lower than the Fermi level of all surfaces under study (both the sample of interest and reference samples). This condition is fulfilled, e.g., in the measurement of the composition of the CuAu(100) surface by means of Na^+ ions [98]. This condition will hold for most metallic surfaces when using K^+ ions (ionization energy 4.34 eV) or Cs^+ ions (ionization energy 3.89 eV). However, the use of relatively heavy K^+ ions substantially reduces the sensitivity of the LEIS method to light elements.

If the neutralization effect cannot be disregarded, there are two ways to consider it:

(1) Correction of data obtained by the method of reference samples.

(2) Direct calculation of elemental sensitivity.

4.1.4.1 Correction of data obtained by the method of reference samples. Let us recall that the surface concentration of element N_i is expressed as

$$N_i = \frac{S_i/\eta_i}{\sum_j S_j/\eta_j}\,, \tag{18}$$

where S_i is the scattering signal of the element i, and η_i is the elemental sensitivity measured on a reference sample.

With the neutralization taken into account, expression (18) is transformed into the following form:

$$N_i = \frac{\left(S_i/P^+_{i,\,\mathrm{sample}}(E,\theta,\varphi)\right)/\left(\eta_i/P^+_{i,\,\mathrm{reference}}(E,\theta,\varphi)\right)}{\sum_j \left(S_j/P^+_{j,\,\mathrm{sample}}(E,\theta,\varphi)\right)/\left(\eta_j/P^+_{j,\,\mathrm{reference}}(E,\theta,\varphi)\right)}\,, \tag{19}$$

where $P^+_{i,\,\mathrm{sample}}(E,\theta,\varphi)$ and $P^+_{i,\,\mathrm{reference}}(E,\theta,\varphi)$ are the probabilities of preserving the positive charge state by the ion upon scattering from the surface of the sample under study and from the surface of the reference sample, respectively.

Probability $P^+(E,\theta,\varphi)$ can be estimated using the available experimental data or calculated. Examples of correcting the data obtained from reference samples are presented in Section 4.1.3.

4.1.4.2 Direct calculation of elemental sensitivity. In this case, the values of elemental sensitivity to be used in expression (18) are calculated as

$$\eta_i = P_i^+(E,\theta,\varphi)\,\frac{\mathrm{d}\sigma_i}{\mathrm{d}\Omega}\,, \tag{20}$$

where the scattering differential cross section $\mathrm{d}\sigma_i/\mathrm{d}\Omega$ is calculated by the pair collision method, and the probability $P_i^+(E,\theta,\varphi)$ of preserving the positive charge state is calculated according to Ref. [99]. It should be noted that ions scattered from different chemical elements will have different velocities, so that $P_i^+(E,\theta,\varphi)$ will depend on the type of scattering element.

Note that the direct calculation of the elemental sensitivity allows reducing by three or more times the number of experiments necessary to determine the surface concentration of chemical elements by LEIS.

4.2 Comparison of low-energy ion scattering with other methods of surface investigation

To date, there are no universal methods of surface diagnostics; therefore, in practice, LEIS is often used in combination [100] with Auger electron spectroscopy (AES) [101–103], X-ray photoelectron spectroscopy (XPS) [104], and time-of-flight secondary ion mass spectrometry (TOF-SIMS) [105]. Each of these methods has certain advantages, and their combination allows receiving more complete information about the surface and surface processes. The main characteristics of LEIS, XPS, AES, and TOF-SIMS methods are summarized in Table 3.

A comparison shows that the key advantages of the LEIS method are high surface sensitivity and accuracy of quantitative chemical composition analysis. LEIS is the only method allowing the determination of the chemical composition of the uppermost surface layer. One more LEIS advantage is the relatively fast performance of experiments and interpretation of their results, which allows studying the dynamics of surface chemical composition variation.

4.3 Examples of practical use of the low-energy ion scattering method

The high surface sensitivity and fast measurements determine the application of LEIS in areas where it is necessary to know

Table 3. Comparison of performance characteristics of LEIS, XPS, AES, and TOF-SIMS methods. Data on LEIS, XPS, and TOF-SIMS are borrowed from review [15]. Data on AES are borrowed from [101–104].

Characteristics	LEIS	XPS	AES	TOF-SIMS
Surface sensitivity	Uppermost layer	3–10 nm	3–10 nm	> 1 nm
Matrix effects	Virtually none	Virtually none	Present	Strong
Quantitative analysis	Possible, high accuracy	Possible, medium accuracy	Possible, medium accuracy	Possible, low accuracy
Information of chemical bonds and degree of oxidation	No	Yes	Yes	Analysis of molecular fragments
Lateral resolution	~ 10 μm	~ 10 μm	~ 10 nm	< 1 μm
Cost of equipment	\$1 million	\$500,000	\$500,000	\$1 million

the surface composition and to follow the surface processes. Note that in complex materials the surface chemical composition may greatly differ from the bulk one, which affects the functional properties of the surface. Examples of practical tasks whose solution requires the LEIS method are the investigation of surface composition of catalysts, the analysis and improvement of catalysis [106, 107], the study of diffusion in thin-film structures of semiconductor devices and the surface composition of fuel cells, as well as all other problems requiring the determination of the composition of the uppermost layer.

4.3.1 Investigation of surface composition of catalysts and surface reactivity. Heterogeneous catalysis, in which the catalyst and reagents are in different phase states, has a number of advantages and is widely used in technological processes. As a rule, the role of catalyst is played by the surface of a solid. The chemical composition and structure of the surface determine its catalytic properties. The LEIS method is necessary to measure the surface elemental composition.

As an example, let us consider the $(Rh_{2-y}Cr_yO_3)/GaN$ surface, which is used to split water into H_2 and O_2 [108]. The pure GaN surface has no catalytic properties. Using a layer-by-layer analysis [2] of the composition by the LEIS method, it was found that the surface layer of this catalyst consists presumably of GaO_x oxide, the near-surface region — of GaO_xN_y, and the bulk — of GaN. It follows that the nitrogen atoms are almost absent on the surface and take no part in the catalysis. Using the layer-by-layer analysis, the profiles of Cr and Rh depth distribution were also determined (Fig. 17). Based on these measurements, the enrichment of the near-surface region [3] by Cr and Rh atoms was demonstrated. Along with this, the experimental value of Rh concentration made it possible to calculate the number of H_2 molecules produced per unit time.

Exchange of electrons between ions and a surface not only is important for diagnosing the surface composition of the catalyst by the LEIS method, but can also be used to estimate the surface catalytic activity [109]. The resonant electron transfer during the neutralization of alkali metal ions on metallic surfaces occurs near the Fermi level of the metal and has a number of mutual properties with the charge transfer in chemical reactions. The surface reactivity strongly depends on the processes of exchanging electrons with the neighboring molecules/atoms/ions [110, 111]. The neutralization during

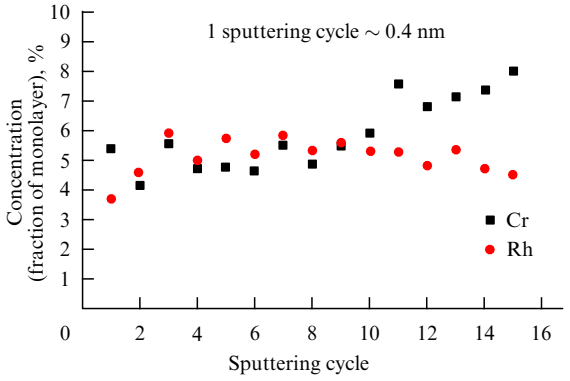

Figure 17. Cr and Rh concentration distribution with respect to sample depth [108]. The description of the catalyst surface under study is given in the text.

low-energy ion scattering is sometimes considered a simplified model for analyzing the factors affecting the rate of chemical reactions on a surface [109]. Advantages of LEIS in reactivity studies are the possibility of varying the interaction time by changing the beam energy and, thus, tracing the dynamics of the electronic transition process, as well as of measuring directly the probability of electron exchange with various atoms of the catalyst surface.[4]

As an example, let us consider gold nanoclusters, which possess unique properties [112]. Macroscopic gold is an inert metal, but nanoclusters of gold manifest a high catalytic capacity, e.g., can efficiently catalyze the oxidation of CO and hydrocarbons [113, 114]. The maximum catalytic activity is manifested by clusters having dimensions of the order of 3 nm [114]. The catalytic activity of clusters depends not only on their size, but also on their shape [115]. To understand the fundamentals of gold nanocluster catalytic capacity, it is necessary to know their local electronic structure and surface reactivity [116–119]. It is noteworthy that the catalytic capacity of gold nanoclusters correlates with the ion neutralization probability: in LEIS experiments, a strong increase (by an order of magnitude) in the probability of alkali metal ion neutralization on gold nanoclusters, as compared to the case of a bulk Au sample [30, 61, 109, 120–123], was found. For example, the neutralization probability for Na scattered from a gold nanocluster with a radius of 1 nm is about 50%, whereas for a bulk sample of gold it is about 3%. Earlier, several possible explanations of this effect were proposed:

[2] For layer-by-layer analysis with the LEIS method, the sputtering of the surface with an ion beam is used.

[3] In comparison with their bulk concentration.

[4] It is possible by separating the scattering signal from different atoms according to the value of energy losses.

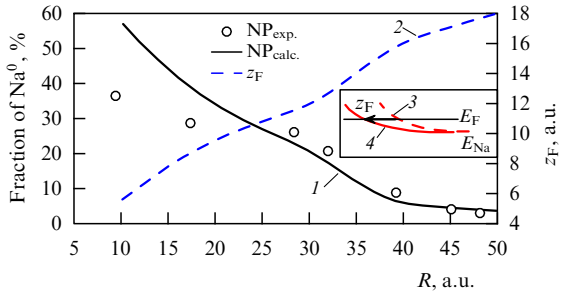

Figure 18. Na^+ ion neutralization probability as a function of Au nanocluster radius (left-hand ordinate axis). Primary beam energy: 2 keV, scattering angle: 150°. Experimental data (black circles) were taken from [120], calculation results — black solid line (*1*) — from [124]. The blue dashed line (*2*) shows the dependence of z_F on the cluster radius (right-hand ordinate axis). The inset illustrates the decrease in z_F due to the 'lowering' of the ion energy position; the red dashed line (*3*) is the energy position $E_a(z)$ of the ion near the solid planar metallic surface; the red solid line (*4*) is taken near a metallic nanocluster; the solid black line is the Fermi level E_F.

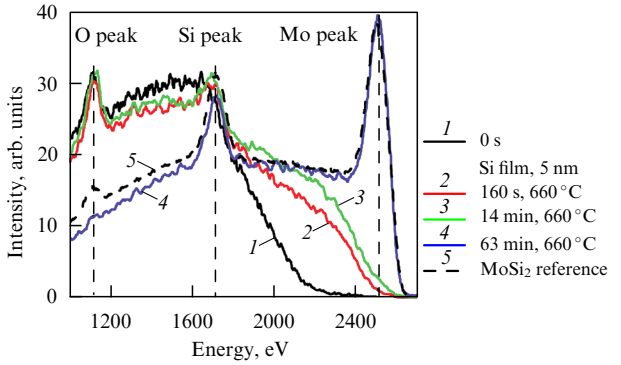

Figure 19. (Color online.) Elemental composition evolution of Si/Mo sample surface (see description in the text) due to Mo diffusion onto the surface at the temperature of 660 °C. Energy spectra of the scattered He^+ ions with an energy of 3 keV are shown at different moments of time (see legend), and the peaks corresponding to scattering from different elements are marked [125].

(1) the smaller work function in small clusters; (2) the effect of cluster charging; (3) the surface roughness; (4) the discreteness of the local electronic structure. However, these factors are unable to explain quantitatively so great an increase in the neutralization probability, and the proposed hypotheses explaining the increase in the neutralization probability were semiempirical.

The existing theoretical basis for calculating neutralization probabilities was completed in [124]. For alkali metal ions, the neutralization is implemented via resonant electron tunneling. The neutralization probability critically depends on the distance z_F of the intersection between the ion energy position and the Fermi level of the metal. It was shown that, due to the decrease in the force of interaction with the image charge, the ion energy position near a metallic nanocluster 'shifts' down relative to the case of a solid planar metallic surface. This leads to a decrease in the intersection distance z_F and a significant increase in neutralization probability (see Section 2.1.3.5). The calculated dependence of Na^+ neutralization probability on the cluster radius is in good agreement with experimental data (Fig. 18).

Thus, a probable explanation of catalytic activity in gold nanoclusters was given by considering the resonant electron transfer during ion neutralization.

4.3.2 Investigation of diffusion in thin-film structures of semiconductor devices. Due to sequential miniaturization of the elemental base, up-to-date semiconductor devices are manufactured using 22-, 10-, and even 7-nm technologies. The sizes of film structures, e.g., a sub-gate oxide, in such semiconductor devices amount to a few nanometers. This is less than the surface sensitivity of such diagnostic methods as XPS, AES, and TOF-SIMS, which makes the LEIS method necessary to explore the elemental composition and processes in thin-film structures. A characteristic example of such processes is the diffusion of atoms from the adjacent regions, which affects the functional properties of semiconductor devices.

As an example of LEIS application, let us consider the study of diffusion in the Mo/Si structures used in UV optics [125]. Using the LEIS method, samples consisting of Mo coated with an Si film of known thickness from 4 to 7 nm were studied. Under heating, the diffusion of Mo atoms onto the sample surface was activated. Figure 19 shows the spectra of He^+ ions with an energy of 3 keV, scattered from the surface under study. From the energy losses, it is possible to identify the scattering peaks produced by different atoms (see Fig. 19). The surface Mo peak is seen to appear only after a certain time. Using LEIS measurements, the diffusion rate and the stopping power $S_{Si} = 36 \pm 3$ eV nm^{-1} of silicon were determined. Note that the fast processing of the results of LEIS measurements allows exploring the diffusion process in real time.

4.3.3 Investigation of the surface composition of fuel cells. Fuel cells are used in space technologies, in stationary power stations, as autonomous sources of heat and electric power supply for buildings, in vehicle engines, and as power supplies in electronic devices [126]. Notably, recently, the technology of solid oxide fuel cells has been undergoing development [127]. In such fuel cells, electricity is produced as a result of the oxidation chemical reaction on a surface. Naturally, knowledge of surface structure is important to analyze the functioning and performance improvement of fuel cells.

As an example of the LEIS method application, let us consider the surface of the $La_{2-x}Sr_xNiO_{4+\delta}$ material, which is promising for exploitation at mean temperatures of 650–800 °C [128]. Note that earlier the composition of this surface was unknown and only numerically modeled, with the results predicting the predominance of nickel oxide on the surface. However, the experimental study of surface composition by the LEIS method demonstrated the absence of an Ni peak (Fig. 20), whereas the La and Sr peaks are clearly seen in the spectrum. Thanks to these measurements, for further studies of the $La_{2-x}Sr_xNiO_{4+\delta}$ material, an alternative model has been chosen, in which the surface consists of La and Sr oxides. Note that from the point of view of numerical modeling, the chosen alternative model is less likely.

5. Conclusion

This review generalizes present-day experimental and theoretical knowledge about resonant electron exchange — the dominant process of charge transfer between atomic particles and metallic surfaces.

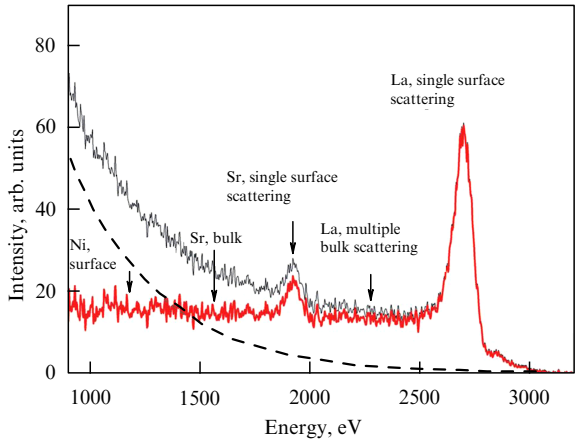

Figure 20. Spectrum of Ne^+ ions with an energy of 5 keV scattered from the surface of a fuel cell (see the description in the text) [128]. Peaks of scattering on various elements are marked.

The main method of experimental study of electron exchange is to analyze the probability of changing the charge state during low-energy ion scattering. Some important information can be obtained using scanning tunneling microscopy/spectroscopy. The existing model representations and approaches to the computational-theoretical description of electron transfer, such as the Anderson–Newns model and the wave packet propagation method, in most cases quantitatively reproduce and explain the experimental regularities.

As the most interesting results, we would like to mention the following: (1) the change in the electron exchange character for surfaces with restricted motion of an electron; (2) the kinematic electron exchange effect; (3) the influence of the discrete structure and restricted dimensions of nanosystems on the electron exchange efficiency; (4) the local aspects of electron exchange in the presence of defects and adsorbates on the surface.

In applications, the electron exchange between atomic particles and surfaces is used for diagnosing the surface composition and creating high-efficiency sources of negative ions. In the diagnostics of surface composition by the method of low-energy ion scattering, the neutralization probability incorrectly accounted for results in errors by a few times in the determination of element concentrations. This is important, because low-energy ion scattering is the only method by which the concentration of chemical elements can be measured in the uppermost layer. High surface sensitivity and speed of measurements allow the application of low-energy ion scattering in areas where it is necessary to know the surface composition and to trace the processes that occur on the surface, including the study of surface composition of catalysts, solid-state fuel cells, and the study of diffusion in thin-film structures of semiconductor devices.

Prospects for further study of electron exchange between ion beams and surfaces are related to experimental and theoretical investigations of more complex systems, including dielectric and semiconductor surfaces, consideration of multielectron charge transfer effects, and diagnostics of properties of functional coatings, which are of practical interest.

The author thanks his colleagues at Lomonosov Moscow State University. Some calculations were performed on the Lomonosov supercomputer in the Research Computing Center of Moscow State University.

References

1. Martynenko Yu V *Sov. Phys. Solid State* **6** 1581 (1965); *Fiz. Tverd. Tela* **6** 2003 (1964)
2. Yurasova V E et al. *JETP Lett.* **21** 88 (1975); *Pis'ma Zh. Eksp. Teor. Fiz.* **21** 197 (1975)
3. Kurnaev V A, Mashkova E S, Molchanov V A *Otrazhenie Legkikh Ionov ot Poverkhnosti Tverdogo Tela* (Reflection of Light Ions from the Surface of a Solid) (Moscow: Energoatomizdat, 1985)
4. Brako R, Newns D *Rep. Prog. Phys.* **52** 655 (1989)
5. Urazgil'din I F *Phys. Rev. B* **47** 4139(R) (1993)
6. Hecht T et al. *Phys. Rev. Lett.* **84** 2517 (2000)
7. Elovikov S S et al. *Bull. Russ. Acad. Sci. Phys.* **66** 608 (2002); *Izv. Ross. Akad. Nauk Ser. Fiz.* **66** 558 (2002)
8. Los J, Geerlings J J C *Phys. Rep.* **190** 133 (1990)
9. Chakraborty H, Niederhausen T, Thumm U *Phys. Rev. A* **70** 052903 (2004)
10. Karaseov P A et al. *Semiconductors* **48** 446 (2014); *Fiz. Tekh. Poluprovodn.* **48** 462 (2014)
11. Andrianova N N et al. *J. Synch. Investig. X-Ray Synchrotron Neutron Tech.* **10** 412 (2016); *Poverkhnost'. Rentgen. Sinkhrotron. Neitron. Issled.* (4) 51 (2016)
12. Shaw J et al. *Phys. Rev. A* **98** 052705 (2018)
13. Winter H *Phys. Rep.* **367** 387 (2002)
14. Brongersma H H et al. *Surf. Sci. Rep.* **62** 63 (2007)
15. Cushman C V et al. *Anal. Methods* **8** 3419 (2016)
16. Stückelberg E C G *Helv. Phys. Acta* **5** 369 (1932)
17. Taglauer E et al. *Phys. Rev. Lett.* **45** 740 (1980)
18. Boers A L *Nucl. Instrum. Meth. Phys. Res. B* **2** 353 (1984)
19. Shen Y G et al. *Surf. Sci.* **328** 21 (1995)
20. Shen Y G et al. *Surf. Sci.* **357–358** 921 (1996)
21. Gadzuk J W *Surf. Sci.* **6** 133 (1967)
22. Gadzuk J W *Surf. Sci.* **6** 159 (1967)
23. Ray R, Mahan G D *Phys. Lett. A* **42** 301 (1972)
24. Arnau A et al. *Surf. Sci. Rep.* **27** 113 (1997)
25. Maazouz M et al. *Phys. Rev. B* **55** 13869 (1997)
26. Delos J B *Rev. Mod. Phys.* **53** 287 (1981)
27. McDaniel E W, Mitchell J B A, Rudd M E *Atomic Collisions: Heavy Particle Projectiles* (New York: Wiley, 1993)
28. Kaempffer F A *Concepts in Quantum Mechanics* (New York: Academic Press, 1965)
29. Burgdörfer J, in *Review of Fundamental Processes and Applications of Atoms and Ions* (Ed. C D Lin) (Singapore: World Scientific, 1993) p. 517
30. Balaz S, Yarmoff J A *J. Phys. Condens. Matter* **22** 084009 (2010)
31. Gao L et al. *Phys. Rev. A* **96** 052705 (2017)
32. Zimny R *Surf. Sci.* **233** 333 (1990)
33. Geerlings J J C, Kwakman L F Tz, Los J *Surf. Sci.* **184** 305 (1987)
34. García E A et al. *Surf. Sci.* **603** 597 (2009)
35. Rau E I et al. *Phys. Solid State* **59** 1526 (2017); *Fiz. Tverd. Tela* **59** 1504 (2017)
36. Hecht T et al. *Faraday Discuss.* **117** 27 (2000)
37. Canário A R et al. *Phys. Rev. B* **71** 121401(R) (2005)
38. Gainullin I K *Phys. Rev. A* **95** 052705 (2017)
39. Ermoshin V A, Kazansky A K *Phys. Lett. A* **218** 99 (1996)
40. Borisov A G, Kazansky A K, Gauyacq J P *Phys. Rev. Lett.* **80** 1996 (1998)
41. Gauyacq J P et al. *Faraday Discuss.* **117** 15 (2000)
42. Gauyacq J P, Borisov A G, in *Quantum Dynamics of Complex Molecular Systems* (Springer Series in Chemical Physics, Vol. 83, Eds D A Micha, I Burghardt) (Berlin: Springer, 2007) p. 87
43. Bardsley J N *Pseudopotentials in Atomic and Molecular Physics* (Pittsburgh: Univ. of Pittsburgh, 1974); in *Case Studies in Atomic Physics 4* (Eds E W McDaniel, M R C McDowell) (Amsterdam: Elsevier, 1975) p. 299
44. Cohen J S, Fiorentini G *Phys. Rev. A* **33** 1590 (1986)
45. Jennings P J, Jones R O, Weinert M *Phys. Rev. B* **37** 6113 (1988)
46. Chulkov E V, Silkin V M, Echenique P M *Surf. Sci.* **437** 330 (1999)
47. Gainullin I K, Sonkin M A *Comput. Phys. Commun.* **188** 68 (2015)
48. Gainullin I K *Comput. Phys. Commun.* **210** 72 (2017)

49. Gainullin I K *Phys. Rev. A* **100** 032712 (2019)
50. Guillemot L, Esaulov V A *Phys. Rev. Lett.* **82** 4552 (1999)
51. Bahrim B, Makarenko B, Rabalais J W *Surf. Sci.* **594** 62 (2005)
52. Canário A R, Kravchuk T, Esaulov V A *New J. Phys.* **8** 227 (2006)
53. Nordlander P, Tully J C *Phys. Rev. Lett.* **61** 990 (1988)
54. Newns D M et al. *Phys. Scripta* **1983** (T6) 5 (1983)
55. Obreshkov B, Thumm U *Phys. Rev. A* **87** 022903 (2013)
56. Borisov A G, Teillet-Billy D, Gauyacq J P *Phys. Rev. Lett.* **68** 2842 (1992)
57. Shestakov D K et al. *Nucl. Instrum. Meth. Phys. Res. B* **267** 2596 (2009)
58. Meyer C et al. *Phys. Rev. A* **86** 032901 (2012)
59. Li J et al. *Surf. Sci.* **422** 95 (1999)
60. Thumm U, Kürpick P, Wille U *Phys. Rev. B* **61** 3067 (2000)
61. Canário A R, Esaulov V A *J. Chem. Phys.* **124** 224710 (2006)
62. Gainullin I K, Urazgildin I F *Phys. Rev. B* **74** 205403 (2006)
63. Gainullin I K et al. *Vacuum* **72** 263 (2003)
64. Gainullin I K, Usman E Yu, Urazgil'din I F *Nucl. Instrum. Meth. Phys. Res. B* **232** 22 (2005)
65. Amanbaev E R et al. *Thin Solid Films* **519** 4737 (2011)
66. Gainullin I K, Sonkin M A *Phys. Rev. A* **92** 022710 (2015)
67. Li J et al. *Science* **299** 864 (2003)
68. Cho A *Science* **299** 36 (2003)
69. Lad R J *Surf. Rev. Lett.* **02** 109 (1995)
70. Azad A M et al. *J. Electrochem. Soc.* **139** 3690 (1992)
71. Kirner U et al. *Sensors Actuators B* **1** 103 (1990)
72. Ilin A S et al. *Sci. Rep.* **7** 12204 (2017)
73. Canário A R et al. *Surf. Sci.* **547** L887 (2003)
74. Usman E Yu et al. *Phys. Rev. B* **64** 205405 (2001)
75. Gainullin I K *Moscow Univ. Phys. Bull.* **74** 585 (2019); *Vestn. Mosk. Gos. Univ. Ser. 3. Fiz. Astron.* (6) 33 (2019)
76. Taylor M, Nordlander P *Phys. Rev. B* **64** 115422 (2001)
77. Binnig G et al. *Phys. Rev. Lett.* **49** 57 (1982)
78. Yaminsky I V (Ed.) *Scanning Probe Microscopy of Biopolymers* (Scanning Probe Microscopy, Issue 1) (Moscow: Scientific World, 1997)
79. Barke I, Hövel H *Phys. Rev. Lett.* **90** 166801 (2003)
80. Gauyacq J P, Borisov A G *J. Phys. Condens. Matter* **10** 6585 (1998)
81. Gauyacq J P, Borisov A G, Bauer M *Time-Resolved Photoemission from Solids: Principles and Applications* (Berlin: Springer, 2005)
82. Scheffler M, Stampfl C, in *Electronic Structure* (Handbook of Surface Science, Vol. 2, Eds K Horn, M Scheffler) (Amsterdam: Elsevier, 2000) p. 285
83. Zimny R, Nienhaus H, Winter H *Vacuum* **41** 359 (1990)
84. Obreshkov B, Thumm U *Phys. Rev. A* **74** 012901 (2006)
85. Obreshkov B, Thumm U *Phys. Rev. A* **87** 022903 (2013)
86. Sereda I et al. *Vacuum* **162** 163 (2019)
87. ter Veen H R J et al. *Catal. Today* **140** 197 (2009)
88. Shen Y G et al. *Surf. Sci.* **328** 21 (1995)
89. Brongersma H H et al. *Platin. Met. Rev.* **54** (2) 81 (2010)
90. Niehus H *Surf. Sci. Lett.* **166** L107 (1986)
91. Van den Berg J A, Armour D G *Vacuum* **31** 259 (1981)
92. Heiland W, Taglauer E *Nucl. Instrum. Meth.* **132** 535 (1976)
93. Robinson M T *Phys. Rev.* **179** 327 (1969)
94. Primetzhofer D et al. *Nucl. Instrum. Meth. Phys. Res. B* **258** 36 (2007)
95. Kolasinski R D, Whaley J A, Bastasz R *Phys. Rev. B* **79** 075416 (2009)
96. Ho C-S et al. *Surf. Sci.* **617** 192 (2013)
97. Ho C-S et al. *J. Phys. Chem. A* **117** 11684 (2013)
98. Beikler R, Taglauer E *Surf. Sci.* **643** 138 (2016)
99. Gainullin I K *Surf. Sci.* **677** 324 (2018)
100. Óvári L et al. *Surf. Sci.* **566 – 568** 1082 (2004)
101. Oura K et al. *Surface Science. An Introduction* (Advanced Texts in Physics) (Berlin: Springer-Verlag, 2003); Translated into Russian: *Vvedenie v Fiziku Poverkhnosti* (Moscow: Nauka, 2006)
102. Powell C J et al. *J. Electron Spectrosc. Relat. Phenom.* **98** 1 (1999)
103. Mitchell D F, Sproule G I *Surf. Sci.* **177** 238 (1986)
104. Troyan V I et al. *Fizicheskie Osnovy Metodov Issledovaniya Nanostruktur i Poverkhnosti Tverdogo Tela* (Physical Foundations of Methods for Studying Nanostructures and Solid Surfaces) (Ed. V D Borman) (Moscow: MIFI, 2008)
105. Vickerman J C, Briggs D *ToF-SIMS: Surface Analysis by Mass Spectrometry* (Chichester: IM Publ., SurfaceSpectra, 2001)
106. Jansen W P A et al. *J. Catal.* **210** 229 (2002)
107. Thakar N et al. *J. Catal.* **248** 249 (2007)
108. Phivilay S P et al. *J. Phys. Chem. Lett.* **4** 3719 (2013)
109. Shen J et al. *Gold Bull.* **46** 343 (2013)
110. Narayanan R, El-Sayed M A *J. Phys. Chem. B* **107** 12416 (2003)
111. Fan C et al. *Anal. Chem.* **73** 2850 (2001)
112. Haruta M et al. *J. Catal.* **115** 301 (1989)
113. Valden M, Lai X, Goodman D W *Science* **281** 1647 (1998)
114. Lai X et al. *Prog. Surf. Sci.* **59** 25 (1998)
115. Narayanan R, El-Sayed M A *J. Am. Chem. Soc.* **126** 7194 (2004)
116. Hagenbach G, Courty Ph, Delmon B *J. Catal.* **31** 264 (1973)
117. Block J H, Kreuzer H J, Wang L C *Surf. Sci.* **246** 125 (1991)
118. Wang A-Q et al. *J. Catal.* **233** 186 (2005)
119. Stamenkovic V R et al. *Nat. Mater.* **6** 241 (2007)
120. Liu G F, Sroubek Z, Yarmoff J A *Phys. Rev. Lett.* **92** 216801 (2004)
121. Liu G F et al. *J. Chem. Phys.* **125** 054715 (2006)
122. Shen J et al. *J. Phys. Chem. C* **119** 15168 (2015)
123. Salvo C, Karmakar P, Yarmoff J *Phys. Rev. B* **98** 035437 (2018)
124. Gainullin I K *Surf. Sci.* **681** 158 (2019)
125. de Rooij-Lohmann V I T A et al. *Appl. Phys. Lett.* **94** 063107 (2009)
126. Bagotzky V S, Osetrova N V, Skundin A M *Russ. J. Electrochem.* **39** 919 (2003); *Elektrokhim.* **39** 1027 (2003)
127. Stambouli A B, Traversa E *Renew. Sustain. Energy Rev.* **6** 433 (2002)
128. Burriel M et al. *Energy Environ. Sci.* **7** 311 (2014)